AD-A120 919 AMORPHOUS IRON BORIDES: PREPARATION STRUCTURE AND MAGNETIC PROPERTIES(U) JOHNS HOPKINS UNIV LAUREL MD APPLIED PHYSICS LAB K MOORJANI 28 SEP 82 1/1

UNCLASSIFIED ARO-15344.6-PH DRXRO-15344-P F/G 11/6 NL

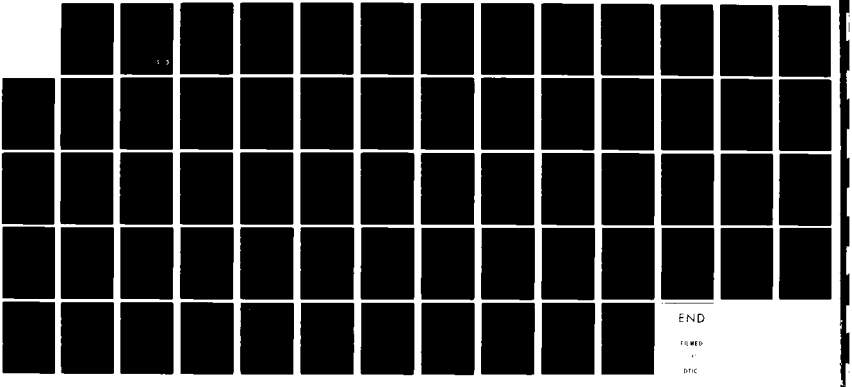

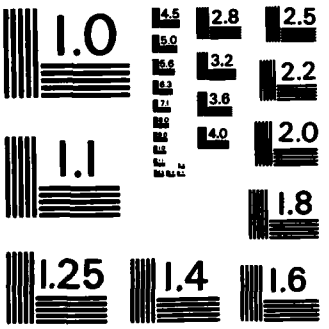

MICROCOPY RESOLUTION TEST CHART
NATIONAL BUREAU OF STANDARDS - 1963 - A

ARO 15344.6-PH

(12)

AMORPHOUS IRON BORIDES: PREPARATION, STRUCTURE AND MAGNETIC PROPERTIES

FINAL REPORT

Kishin Moorjani

September 1982

U. S. ARMY RESEARCH OFFICE

Contract DRXRO-15344-P

The Applied Physics Laboratory
The Johns Hopkins University
Laurel, Maryland 20707

UNCLASSIFIED

SECURITY CLASSIFICATION OF THIS PAGE (When Data Entered)

REPORT DOCUMENTATION PAGE		READ INSTRUCTIONS BEFORE COMPLETING FORM
1. REPORT NUMBER	2. GOVT ACCESSION NO. AD-A120 919	3. RECIPIENT'S CATALOG NUMBER
4. TITLE (and Subtitle) AMORPHOUS IRON BORIDES: PREPARATION, STRUCTURE AND MAGNETIC PROPERTIES		5. TYPE OF REPORT & PERIOD COVERED Final - 11/78 to 6/82
		6. PERFORMING ORG. REPORT NUMBER
7. AUTHOR(s) Kishin Moorjani		8. CONTRACT OR GRANT NUMBER(s) DRXRO-15344-P
9. PERFORMING ORGANIZATION NAME AND ADDRESS The Applied Physics Laboratory The Johns Hopkins University Laurel, Maryland 20707		10. PROGRAM ELEMENT, PROJECT, TASK AREA & WORK UNIT NUMBERS
11. CONTROLLING OFFICE NAME AND ADDRESS U. S. Army Research Office Post Office Box 12211 Research Triangle Park, NC 27709		12. REPORT DATE 28 September 1982
		13. NUMBER OF PAGES 65
14. MONITORING AGENCY NAME & ADDRESS(if different from Controlling Office)		15. SECURITY CLASS. (of this report) Unclassified
		15a. DECLASSIFICATION/DOWNGRADING SCHEDULE NA

16. DISTRIBUTION STATEMENT (of this Report)

Approved for public release; distribution unlimited.

17. DISTRIBUTION STATEMENT (of the abstract entered in Block 20, if different from Report)

NA

18. SUPPLEMENTARY NOTES

The view, opinions, and/or findings contained in this report are those of the author(s) and should not be construed as an official Department of the Army position, policy, or decision, unless so designated by other documentation.

19. KEY WORDS (Continue on reverse side if necessary and identify by block number)

amorphous metals, tailoring of materials, rapid solidification technology, magnetic properties, structure of amorphous alloys, iron borides

20. ABSTRACT (Continue on reverse side if necessary and identify by block number)

Chemically and magnetically homogenous samples of amorphous iron-boron alloys over a wide concentration range have been fabricated and examined for their atomic and magnetic structures. The knowledge of homogeneity is important in obtaining controllable materials for device applications, and the determination of atomic structure, distribution of magnetic moments and isomer shift is essential to the knowledge of chemical short-range order and the direction and amount of charge transfer. The details of these measurements along with their interpretation and formulation of theoretical models are described.

DD FORM 1 JAN 73 1473 EDITION OF 1 NOV 65 IS OBSOLETE

UNCLASSIFIED

SECURITY CLASSIFICATION OF THIS PAGE (When Data Entered)

Foreword

Amorphous metallic alloys possess attractive and unexpected metallurgical, mechanical, and magnetic properties which have led to exciting possibilities ranging from materials developments and substitutions for scarce and strategic materials, to applications in electromagnetic machinery and electronic devices. The key to fabricating these materials lies in rapid solidification technology which offers better homogeneity and better structural refinement of materials. The possibility of tailoring the structure and composition and hence the behavior of amorphous alloys offers an enormous advantage over crystalline solids. The details of tailoring depend crucially on a number of fundamental concepts such as the nature of bonding and the degree of local atomic order which in turn affect the electronic band structure and therefore the physical properties.

Over the past three and one-half years, we have made substantial progress towards obtaining a basic understanding of disorder induced changes on the magnetic properties of amorphous alloys. The prototype materials in our investigation were the binary iron-boron alloys chosen for their relative simplicity and their importance in elucidating charge transfer processes. Chemically and magnetically homogeneous samples over a wide concentration range have been fabricated and examined for their atomic and magnetic structures. The knowledge of homogeneity is important in obtaining controllable materials for device applications, and the determination of atomic structure, distribution of magnetic moments and isomer shift is essential to the knowledge of chemical

short-range order and the direction and amount of charge transfer. The details of these measurements along with their interpretation and formulation of theoretical models are described in the next section.

TABLE OF CONTENTS

Page

I. Measurements and Results.....1

A. Specimen Preparation.....1

B. Secondary Ion Mass Spectrometer (SIMS).....1

C. X-Ray Diffraction Studies.....3

D. Mössbauer Studies.....5

E. Ferromagnetic Resonance.....10

F. Theoretical Modeling.....13

II. Summary of Important Results.....34

III. Publications.....36

IV. Participating Scientific Personnel.....37

V. References.....38

Figures.....19

Table I.....33

Appendices.....40

LIST OF APPENDICES, ILLUSTRATIONS, AND TABLES

APPENDICES

APPENDIX 1

K. Moorjani, S. K. Ghatak, K. V. Rao, B. Kramer, and H. S. Chen, "Spin Glass - Paramagnetic Phase Boundary in Amorphous Magnetic Alloys," J. Phys. (Paris), Colloquia C8, C8-718 (1980).

APPENDIX 2

N. A. Blum, K. Moorjani, T. O. Poehler, and F. G. Satkiewicz, "Hyperfine Field Distributions in Ferromagnetic Amorphous Fe_xB_{1-x} Thin Films," J. Appl. Phys. 52, 1808 (1981).

APPENDIX 3

N. A. Blum, K. Moorjani, T. O. Poehler, and F. G. Satkiewicz, "Mössbauer Investigation of Sputtered Ferromagnetic Amorphous Fe_xB_{100-x} Films," J. Appl. Phys. 53, 2074 (1982).

APPENDIX 4

D. J. Webb, S. M. Bhagat, K. Moorjani, T. O. Poehler, and F. G. Satkiewicz, "Spin Glass Behavior and Non-Ergodicity in Amorphous Iron-Boron Alloys," Solid State Comm. 43, 239 (1982).

APPENDIX 5

N. A. Blum, "Mössbauer Study of Magnetism in an Amorphous $Fe_{40}B_{60}$ Sputtered Film," J. Appl. Phys. (to be published, 1983).

FIGURES

1. Variations with depth in iron stoichiometry in a typical sputtered Fe-B film (#22 on glass); average atomic fraction of iron: 0.514±0.004.

2. Energy dispersive X-ray diffraction system.

3. Radial distribution function for a-$Fe_{71}B_{29}$.

4. (a) Spectrum of Fe_2B (powder) compared with (b) spectrum of a-$Fe_{71}B_{29}$ sputtered film.

5. P(H) distributions for a-$Fe_{71}B_{29}$ at 295, 77, and 10 K.

6. Mössbauer spectrum and least squares optimized magnetic hyperfine field distributions P(H) for sputtered amorphous $Fe_{53}B_{47}$ film at T = 295 K.

7. (a) Spectrum of a-$Fe_{40}B_{60}$: H_{app} = 80 kOe, T = 4.2 K. Solid line is theoretical diagmagnetic components. (b) Same as (a) with theoretical spectrum subtracted ("stripped" data). (c) Stripped data with solid line showing spectrum from P(H) fit. (d) P(H) giving best fit to stripped spectrum. Dashed line represents meaningless part of distribution.

8. Temperature dependence of the magnetization deduced from FMR data on amorphous Fe_xB_{1-x} alloys. As described in the text, below 80 K, Fe_{47} and Fe_{49} do not show simple behavior, hence the dashed lines.

9. Temperature dependence of the FMR linewidths at 11 GHz for amorphous Fe_xB_{1-x} alloys.

10. Temperature dependence of the resonance field for FMR in amorphous Fe_{47}. Below 80 K, the data are dependent upon the thermal history. The solid line is obtained on slow (~0.25 K/min) cooling while the other data represent other thermal cycles.

11. Magnetic phase diagram for the alloy $(A_xB_{1-x})_cD_{1-x}$; T_c and T_n are normalized Curie and Néel temperatures. For definition of other parameters, see text.

12. Magnetic phase diagram for the alloy $(A_xB_{1-x})_cD_{1-c}$; T_c and T_n are normalized Curie and Néel temperatures. For definition of other parameters, see text.

13. Magnetic phase diagram for the alloy $(A_xB_{1-x})_cD_{1-c}$; T_c and T_n are normalized Curie and Néel temperatures. For definition of other parameters, see text.

14. Magnetic phase diagram (schematically) for the model discussed in the text. The three para-spinglass phase boundaries correspond to the greater than (•••••), equal to (-•-•-•) and less than (■-■-■-) signs in Eq. (7).

TABLE

1. Isomer shifts (δ), magnetic ordering temperature (T_c) and value of H for which P(H) is maximum (H_{peak}) for several amorphous alloys, polycrystalline Fe_2B and the metastable phase Fe_3B. Isomer shifts are relative to α-Fe with source and absorber at 300 K.

I. Measurements and Results

A. Specimen Preparation

Amorphous Fe_xB_{100-x} alloys were prepared by sputtering in an 18 inch vacuum system capable of either rf or dc sputtering at power levels of 1 kilowatt. Typical Fe_xB_{100-x} specimens were prepared by rf sputtering of mixed powder targets (Fe_2B, Fe_2B + FeB, FeB or FeB + B) in an inert gas such as argon at partial pressures of approximately 10 μm. A special magnetic focusing ring was used to confine the sputtering ions so as to enhance the sputtering rates. The resulting rates of approximately 50 A/min are customarily used to grow films of 5 to 10 μm thickness as measured by interferometric methods.

Films of a wide composition range have been prepared on substrates including glass, fused quartz, beryllium, and Kapton according to the experiments in progress. Through careful control of deposition parameters, target materials and source holders, conditions were finally achieved that lead to chemically and magnetically homogeneous samples as judged by secondary ion mass spectrometry and ferromagnetic resonance.

B. Secondary Ion Mass Spectrometer (SIMS)

The sputter-ion source secondary ion mass spectrometer at APL is a powerful and unique tool in thin film research and in the study of solids in general. It consists of a high-voltage primary source of inert gas ions which generates secondary ions from a test specimen by ion sputtering. The secondary ions originating from the sample are focused electostatically into a double-focusing mass spectrometer. A

spectrum is obtained by changing the magnetic field at constant accelerating potential. The secondary ions are detected by an ion multiplier with very low background current and recorded on an X-Y chart recorder.

The interaction of the ion beam with the target results in the production of atomic and polyatomic fragments of which an ample fraction are ionized. The rate at which a given material is sputtered can be controlled by varying the beam intensity. When a defocused beam is used with an exit aperture on the einzellens, flat craters in planar samples are produced. This enables one to obtain concentration profiles with depth without a crater shape correction. It is also useful in evaluating variations in composition of films prepared by evaporation or sputtering. An example of the composition variations of a representative Fe-B film prepared by sputtering is shown in Fig. 1.

A study of the initial Secodary Ion Energy Distribution (SIED) for a number of species has shown that, in general, atomic ions have broader distribution curves. Thus, with the window at the lower ion energy portion of the distribution curves, polyatomic as well as atomic species are seen in the mass spectra. On the other hand, when the window is at the higher energy end of the curves, essentially only atomic ions are recorded in the spectra.

Further extended studies of SIED have shown, that for a given element, the SIED depends on the bonding in a specific matrix and that for dopants in glasses, the areas under the SIED curves exhibit a direct relation to the first ionization potential.

The major task in using SIMS for quantitative work is to convert intensities into concentrations. This can only be accomp'ished by protracted studies of sputtering behavior, by having a thorough familiarity with the spectrometer in use, and having access to suitable calibration samples. All of these factors were used in the past contractual period to arrive at an understanding of the conditions required to obtain meaningful compositional analyses.

C. X-ray Diffraction Studies

Atomic structures of non-crystalline solids can be specified with much less precision than those of their crystalline counterparts. For crystals, knowledge of the Bravais lattice and positions of atoms within the unit cell, which can usually be obtained by X-ray diffraction, is sufficient to fix all the atomic positions, at least up to the nearest defects. In non-crystalline solids there is no unit cell, and X-ray diffraction is inherently less informative, providing only a probabilistic distribution function.

Atomic positions in an amorphous solid are far from completely random in the sense that positions of atoms in a gas are random. The fact that a solid is composed of atoms in contact with one another impose some regularity on the local environment of each of them. Atomic positions are strongly correlated in the nearest neighbor shell, yet uncorrelated beyond a few interatomic spacings. This is the meaning of the common statement that amorphous solids possess short-range order but no long range order.

X-ray diffraction patterns for amorphous materials consist of several diffuse intensity peaks rather than the series of sharp diffraction peaks exhibited in the patterns for crystalline materials. It is possible to investigate an amorphous pattern by the methods of Fourier analysis and determine the nature of the sample structure. The lack of any overall structural regularity removes from the X-ray diffraction patterns of such specimens differentiation of the scattering in a directional sense. This has the direct consequence that the available intensity information permits the determination of the magnitudes of the interatomic vectors, but not their directions. The results can be portrayed as a radial distribution function (RDF) of the radial distance from any reference atom in the system. The average number of atoms is given by $4\pi r^2\rho(r)dr$ where r is the radial distance from the origin and $\rho(r)$ is the density fo the atoms. Thus the atomic coordination number as a function of interatomic distance can be determined.

Energy dispersive X-ray diffraction (EDXD) analysis has proved to be a very useful tool in determining the intensity versus energy diffraction patterns for amorphous solids.[1] The energy dispersive instrumentation, shown in Fig. 2, includes a solid state detector and multichannel analyzer. Data acquisition generally takes from five to ten hours and data analysis is performed using a fast Fourier computer routine to transform the corrected diffraction information.

The energy dispersive diffraction system is not affected by fluctuations in the intensity of the source since the counting of all photons is done simultaneously. No mechanically moving parts are involved

so accuracy and reproducibility are higher than for an angular scan diffractometer system. Also, the total intensity of the white radiation is usually higher than the intensity of a characteristic radiation line, resulting in much faster data collection.

During the first phase of the program, an EDXD system complete with data analysis components has been assembled and the radiation distribution functions obtained for a number of amorphous iron-boron alloys deposited on different substances as well as alloys obtained by rapid quenching. Spectra of rapid quenched samples were found to be easier to interpret due to the absence of a substrate. However, specimen deposited on Kapton (duPont polyimide film) in contrast to those on quartz or beryllium, are also easily amenable to data analysis due to lack of interference from substrate. Our recently obtained results on a-$Fe_{71}B_{29}$ are shown in Fig. 3 and are being presently analyzed in terms of a model suggested by our Mössbauer data.

D. Mössbauer Studies

Mössbauer spectroscopy has proved to be an extraordinarily useful tool for investigating magnetic properties and structure of amorphous alloys containing iron as one of the elemental constituents. Background material on the Mössbauer effect and its application to the study of magnetic materials is well documented elsewhere,[2] and will not be repeated here.

Sputtered films of Fe_xB_{100-x} in the composition range, $40 \leq x \leq 71$, not accessible by melt-quenching techniques were studied. The range

covers the composition corresponding to crystalline compounds FeB,[3] and Fe_2B[4] which facilitates the delineation of disorder induced effects.

Mössbauer spectra were obtained using a ^{57}Co in Rh source at the same temperature as the absorber, except in the 10 K experiments where the source was at room temperature. External magnetic field experiments were performed in a superconducting solenoid with both source and absorber at 4.2 K. The observed broadened magnetic spectra were analyzed using a version of Window's procedure for fitting a continuous distribution of magnetic hyperfine fields to a truncated cosine series expansion of P(H).[5]

Several samples, prepared by sputtering Fe_2B polycrystalline powder from the iron source holder, were determined by SIMS to be homogeneous (to better than ±0.5%) and to have a composition very close to $Fe_{71}B_{29}$. Samples with somewhat less iron content were prepared by sputtering from a mechanical mixture of Fe_2B and FeB. The room temperature spectrum of a typical sample,[6] compared with the spectrum of Fe_2B powder, is shown in Figure 4. Qualitatively, the spectra are similar except for two prominent features which characterize nearly all the ferromagnetic amorphous film spectra: (i) the six lines are broadened in the amorphous alloy, and (ii) the line intensity ratios are quite different in the amorphous film compared with the crystalline powder. The broadened lines of course reflect the non-uniqueness of the hyperfine field, and the line intensity ratios indicate that the iron magnetic moments in the amorphous alloy lie close to the plane of the substrate. In the (randomly oriented) powder, the line intensities are close to the theoret-

ical ratio (3:2:1). In the amorphous alloy the intensity ratios are not immediately evident by inspection because of the distribution of hyperfine fields; however, analysis indicates that the ratio is close to 3:3.5:1 placing the average magnetization direction about 15° out of the plane of the film. The magnetic hyperfine field distributions P(H) are shown in Fig. 5 for various temperatures and are found to shift to higher fields on lowering the temperature. Spectra were also obtained in 50 K increments above room temperature up to 600 K. At 600 K the spectrum is partially collapsed with $H_{peak} \approx 180$ kOe, to be compared with the value of about 250 kOe at 10 K. The result for the magnetic ordering temperature is estimated to be larger than 750 K.

The room temperature parameters of a-$Fe_{71}B_{29}$ are not greatly dissimilar from its crystalline near-counterpart, Fe_2B. The disordered structure of the amorphous alloy causes variations in the magnetic hyperfine fields seen by different Fe atoms. The hyperfine field distribution, depending on the configurations of neighboring magnetic atoms, is centered at a value near the Fe_2B hyperfine field and is rather symmetrically distributed about that value. This is in contrast to results on a-FeB, discussed below, and points towards the existence of similar chemical short range order in amorphous samples with a composition in the vicinity of $Fe_{67}B_{33}$ and crystalline Fe_2B. The results for sputtered $Fe_{71}B_{29}$ are also similar to those for melt-quenched $Fe_{72}B_{28}$,[7] and are shown in Table I along with parameters for Metglas $Fe_{80}B_{20}$ and the metastable phase Fe_3B.

Sputtering pure FeB produced uniform films with a composition $Fe_{53}B_{47}$ as measured by SIMS. Figure 6 shows the room temperature spectrum of $Fe_{53}B_{47}$.[8] Unlike Fe_2B, the amorphous sample spectrum is distinctly different from its crystalline counterpart. The P(H) fit shows a low field component plus a distribution centered around 130 kOe. As the temperature is reduced the spectra show a broadly distributed high magnetic field (~130 kOe) component increasing in both intensity and width. The central peak in the Mössbauer spectrum, indicative of a low or zero field contribution, is present down to 10 K. The P(H) distributions show that the area under the main distribution becomes larger with decreasing temperature and that the peak of this distribution moves toward higher magnetic field. At all temperatures there is a significant peak at low field, encompassing the region approximately 0 to 60 kOe. Mössbauer spectra of amorphous samples with $x \approx 50$ and spectra of $Fe_{53}B_{47}$ at temperatures above room temperature all show a distinct (partially resolved) quadrupole doublet near zero velocity. The quadrupole doublet persists above T_c in all samples, even down to 10 K (above T_c, it is best fit by an equivalent P(H) distribution peaked near 40 kOe with a FWHM of about 40 kOe). The intensity ratio indicate that the average magnetization direction in these samples lies approximately 50° out of the plane of the film.

The Fe atoms in crystalline FeB experience a unique environment with a saturation magnetic hyperfine field of 131 kOe. In order to explain the observed distribution of magnetic hyperfine fields in the amorphous $Fe_{50}B_{50}$ alloys, one must conclude that a large number of Fe

atom environments are very different from the ones in crystalline FeB. The large difference in the values of electric quadrupole splitting (Ref. 9, Table I) also points to the same conclusion, in contrast to the interpretation of experiments on liquid-quenched amorphous $Fe_{75}B_{25}$, where the local chemical order is believed to be the same as that in crystalline Fe_3B.[7,10] The results suggest a structural model for amorphous $Fe_{50}B_{50}$ alloys in which somewhat more than half of the Fe atoms reside in regions having a local chemical order similar to crystalline ferromagnetic FeB, with deviations around the crystalline bond lengths and angles. The remaining non-ferromagnetic Fe sites may lie on the surfaces of, or at interstices between, these regions and thus have local surroundings substantially different from the crystalline ones. The number of these such sites increases with decreasing Fe content.

Since on reducing the iron concentration in samples with 50 ± 10% Fe the "low field bump" in the P(H) distribution increases in amplitude at the expense of the "high field bump" (130 kOe) associated with the ferromagnetic component, it was hoped that there would be little interference in the Mössbauer spectra from the high field component if one studied a sample of sufficiently low iron content to exhibit only the low field P(H) bump. Therefore, a-$Fe_{40}B_{60}$ sample was investigated under a high external magnetic field to reveal the nature of the non-ferromagnetic component. Interpretation of the high field spectra was, however, not as simple as anticipated. This is primarily because at least two, qualitatively distinct, types of magnetic behavior were observed. In order to simplify the spectra a method for subtracting an

observed non-magnetic component from the experimental spectrum was devised. As an example, the H_{app} = 80 kOe experimental spectrum is shown in Figure 7(a) together with a theoretical spectrum (solid line) of just the diamagnetic component. The theoretical spectrum was obtained using "best guesses" for the hyperfine parameters. The method of generating the theoretical spectrum for a mixed electric quadrupole/magnetic dipole interaction is described elsewhere.[11] For the diamagnetic atoms the quantization axis is the external magnetic field direction, and the electric field gradient tensor principal axis is averaged over all directions in computing the theoretical spectrum. Figure 7(b) shows the experimental data after subtracting the diamagnetic spectrum; and Figure 7(c) and 7(d) show the fit (solid line) and P(H) for this "stripped" spectrum. The P(H) peak for the stripped spectrum is nearly independent of the applied field (see Table I of Ref. 8), representing a component in the spectrum that appears to be almost shielded from the external magnetic field. Both this method and the P(H) distribution method were used to analyze the external field data. The results indicate that $Fe_{40}B_{60}$ possesses a complicated magnetic structure which is not yet fully understood.[8]

E. Ferromagnetic Resonance

In the ferromagnetic resonance technique, one measures the absorption of microwave radiation as a function of an applied magnetic field at different orientations of the field with respect to the film plane. The measurements can be carried out at several frequencies and temperatures and when carefully analyzed lead to the knowledge of saturation

magnetization relaxation parameters, and also provide direct evidence for the degree of magnetic inhomogeneity in the film. The later information is not easily accessible from other techniques. The method has recently been exploited to study amorphous magnetic alloys and measurements on our samples have readily established the magnetic homogeneity of these samples as evidenced from the narrow linewidths.

The most detailed FMR measurements have been carried out in samples with x in the vicinity of 0.5.[12] Parallel geometry ($H_{d.c.}$ ∥ to sample plane) was employed at frequencies of approximately 11 GHz and 35 GHz in the temperature range 2-300 K. Using the equation $(\omega/\gamma)^2 = H_r(H_r+4\pi M)$, where H_r corresponds to the field at the resonance center, the H_r data were used to evaluate $4\pi M$ and the results are presented in Fig. 8. Apart from slight deviations below ~20 K, the conventional behavior, $M = M_0(1-BT^{3/2})$, due to excitations of spin waves is a good representation for x = 0.53 over the entire temperature range (i.e., up to T/T_c = 0.54). For alloys with x = 0.49 and 0.47, the $T^{3/2}$ dependence is observed only for $T \gtrsim 80$ K. At lower temperatures, the variation in H_r is quite complex and will be discussed later.

The temperature dependence of the linewidth (Fig. 9) at 11 GHz clearly shows the anomalous behavior at low temperatures. Above approximately 125 K, the linewidth is independent of temperature showing a characteristic ferromagnetic behavior. But at lower temperature, particularly for x = 0.47, linewidth increases rapidly and shows a maximum at ~15 K. This behavior has been interpreted as reentrant ferromagnetism in that the ground state at 0 K is not ferromagnetic but is

instead a spin glass state. Thus, on reducing the temperature, a ferromagnetic-spin glass transition is observed. It is postulated that the spin glass state arises due to the existence of some of the Fe-Fe interactions, either between spins or between clusters of spins that are antiferromagnetic leading to competing exchange and therefore spin glass behavior. Such a possibility had been foreseen in our original proposal[2] and is being fully explored at present.

The anomalies in magnetization mentioned above have been shown to depend on the rate of cooling as illustrated in Fig. 10 for x = 0.47. The solid line is obtained either by cooling slowly (~0.25 K/min) or by cooling in zero field directly to 4 K and observing H_r during a subsequent warming. When the sample is first cooled rapidly (~2 K/min) from 80 K to 50 K, the H_r values represented by solid circles are observed during a subsequent warm-up. The warming could be carried out quite slowly without affecting the H_r data. Yet in another run, the cooling between 80 K and 50 K is accomplished in ten minutes, followed by a slow cool to lower temperatures and the data shown as full squares results.

It is clear that, depending on the cooling rate, the system ends up in different metastable equilibrium states which constitute the local free energy minima. The observation lend credence to the suggestion that the spin glass state is inherently non-ergodic.[13] Many roughly equivalent free energy minima with significant barriers between them exist so that some of the minima are inaccessible during the approach to equilibrium. The system can therefore get locked into a state of "local" equilibrium in which the spin configurations and the consequent

internal fields are quite different from those in the "true" equilibrium state.

F. Theoretical Modeling

In marked contrast to the theoretical results on crystalline solids, little work on amorphous solids is available to explain the existing data or to serve as a useful guide to planning new and definitive experiments. The absence of long range order in the atomic structure introduces immense complexities in the comprehensive theoretical investigation of amorphous solids. It is therefore imperative to analyze relatively simple models which bear enough relationship to actual disordered solids to be able to delineate the disorder induced effects on electronic and magnetic properties. In addition, the analysis of such models serves as a useful guide in interpreting experimental data and fruitful planning of new experiments. We have therefore formulated and analyzed a theoretical model for magnetism in disordered solids which is briefly described below.

Our model concerns systems containing a large concentration of ferromagnetic metallic impurities in a disordered diamagnetic host. It was actually the theoretical modeling that motivated our experimental work on amorphous iron-boron alloys (a-Fe_xB_{100-x}). Such alloys, as already mentioned above, exhibit many interesting properties that should help us to understand phenomena as varied as hopping conduction, insulator-metal transition and magnetic interactions in disordered solids. A site-disordered alloy, A_xB_{1-x}, with concentration x of

magnetic atoms, A, randomly distributed in a nonmagnetic lattice of B atoms with concentration 1-x is considered. The lattice is assumed to be structurally disordered which induces fluctuations in the ferromagnetic exchange interactions between magnetic atoms. Thus, besides the temperature and the coordination number of the lattice, the relevant parameters for the discussion of thermodynamic quantities are the concentration of the magnetic atoms, x, and the measure of fluctuations, Δ. The crystalline ferromagnet results in the limits $x = 1$ and $\Delta = 0$ and serves as a useful check on the calculations performed.

In binary alloys, A_xB_{1-x}, one would observe the onset of ferromagnetism for a critical concentration, x_0, of magnetic atoms. Since the conventional molecular field approximation does not predict a critical concentration, it would not be appropriate for discussion of the properties of A_xB_{1-x} over the entire range of x. We have therefore considered a cluster model and have investigated it within the Bethe-Peierls-Weiss approximation.[14] The resulting free energy is averaged over all the configurations of the disordered system, and a self-consistent condition on magnetization is used to yield expressions for thermodynamic quantities of interest. The procedure allows a systematic investigation of the effect of fluctuations on various thermodynamic variables.

It is shown that the critical concentration, x_0, is not influenced by the presence of fluctuations.[14] This is a reasonable result since it is the presence of a magnetic bond that is important, not its strength. The value of x_0 (= 1/3) is found to be in fair agreement with the exper-

imental value (0.4) deduced from the Curie temperature versus concentration measurements on iron atoms randomly substituted in amorphous germanium.[15] For $x > x_0$, the fluctuations depress the values of the Curie temperature, the high temperature magnetic susceptibility, and the magnetization relative to the corresponding values for the average crystal. For small values of Δ, explicit expressions for the amount of decrease in these quantities are obtained. However, the critical indices for magnetization as well as susceptibility are found to be unaffected by fluctuations.[14]

Although most amorphous solids containing a substantial proportion of magnetic atoms are ordered ferromagnetically, more complex magnetic structures can and do occur. The complexity of the magnetic structure is determined by the crystalline field anisotropy and relative strengths and signs of various magnetic interactions.[16] One such complex magnetic structure, termed "spin glass", possesses no long-range magnetic order but does exhibit anomalies in its thermodynamic behavior.[17] It is expected that a study of spin glasses will answer questions concerning the fundamental nature of exchange interactions.

The above formulation has been modified to discuss the static properties of the Edwards-Anderson Model of a spin glass[18] where exchange interactions are assumed to obey a Gaussian distribution centered at zero. Thus competing exchange interactions occurs with equal probability. In our treatment,[19] the presence of a finite number of nearest neighbors increases the value of the spin glass transition temperature compared to the molecular field result of Edwards and Anderson. Fur-

thermore, in contrast to the molecular field approximation, the magnetic susceptibility approaches the transition temperature from below with a finite positive slope, in agreement with the experimental results.

The model has been further extended to random ternary alloys of the type $(A_xB_{1-x})_cD_{1-c}$ where A and B are magnetic species while D represents the non-magnetic atoms.[20] Such a model allows for competition amongst the three exchange interactions J_{AA}, J_{AB}, and J_{BB}. We have analyzed the model where J_{AA} is taken to be ferromagnetic while J_{BB} is assumed to be antiferromagnetic and the sign of J_{AB} is allowed to vary. The details of the model are being written up for publication and here we only summarize the important results. Depending on the relative concentration of various interactions, various phases are obtained. The equation that determines the complete phase diagram is

$$x\,[(z-1)c^2\,L_{1,2}^2 \mp zcL_{1,2} + 1] + (1-x)[(z-1)c^2\,L_{2,3}^2 \mp zcL_{2,3} + 1] = 0 \qquad (1)$$

where z is the coordination number of the lattice. The upper sign is for the ferromagnetic state while the lower sign is for the antiferromagnetic state and,

$$L_{1,2} = xL_1(y_1) + (1-x)L_2(y_2)$$

and (2)

$$L_{2,3} = xL_2(y_2) + (1-x)L_3(y_3).$$

The L_i's are the Langevin functions and their arguments y_i's are given by $y_i = 2\,J_iS(S+1)/kT$ with $J_1 = J_{AA}$, $J_2 = J_{AB} = J_{BA} = \alpha J_1$ and $J_3 = J_{BB} = \beta J_1$. Thus for a given set of values for (z, c, α, β) one can obtain

$y^{-1}_{1C,N} = kT_{C,N}/2J_1S(S+1)$ as a function of x; $T_{C,N}$ being the Curie or the Néel temperatures. The overall results for a number of parameters are shown in Figs. 11 to 13. For x = 1, the alloy is ferromagnetic and its Curie temeprature T_C is decreased as increasing number of antiferromagnetic bonds are introduced (Fig. 11). The rate of decrease depends on the values of α and β as does the critical concentration at which the ferromagnetic phase disappears (Figs. 12 and 13). The paramagnetic phase prevails until the number of ferromagnetic bonds is large enough to lead to the existence of antiferromagnetic phase above a critical concentration. The Néel temperature then increases with decreasing x as shown in Figs. 11 to 13.

At low temperatures, due to competing exchange interactions, one might expect to obtain the spin glass phase. We have investigated such a behavior for the above model in the limit of large z.[21] The equations determining the phase boundaries are given by,

$$2\langle\xi^2\rangle + 2zq\langle\xi\rangle + 3 = 0 \qquad \text{(ferromagnetic-paramagnetic)} \tag{3}$$

and

$$\langle\xi^2\rangle = 1/2\ (2z^2q^2 - 3) \qquad \text{(paramagnetic-spin glass),} \tag{4}$$

where $q = (3/2z)^{1/2}$, $\xi = J/2kTq = aJ$, and z is the number of nearest neighbors. The configurationally averaged quantities $\langle\xi\rangle$ and $\langle\xi^2\rangle$ are given by

$$\langle\xi\rangle = ay^2J_1^2\ [x^2 + \beta(1-x)^2 + 2x(1-x)] \tag{5}$$

and

$$\langle \xi^2 \rangle = a^2 y^2 J_1^2 [x^2 + \beta^2 (1-x)^2 + 2\alpha^2 x(1-x)]. \qquad (6)$$

The complete phase diagram of the random alloy is determined by Eqs. (3) through (6). The results are depicted in Fig. 14 for y = 1 and z = 8. The important point is that the slope dT_{sg}/dx of the paramagnetic/spin glass phase boundary in the vicinity of x_t, the point where the three phases meet, is positive, zero, or negative depending on whether

$$|\beta| \lessgtr \left(\frac{x_t + \alpha^2 (1-2x_t)}{(1-x_t)} \right)^{1/2}. \qquad (7)$$

These trends have been noticed in a number of amorphous metallic alloys.

Lastly, we mention a recently developed model to understand the dynamics of spin glasses, in particular the temperature dependence of the resonance linewidth. The observed increase in linewidth at low temperatures is seen to be caused by inhomogeneous line broadening due to the existence of random molecular fields. At high temperatures the effect of these fields is negligible due to thermal spin fluctuations. But as temperature decreases the spins with exchange energy greater than the thermal energy start to correlate and produce local fields. As temperature is lowered further, increasing number of spins participate in producing local fields thus increasing the moment of the line shape; the second moment being a direct measure of line broadening. For a spin glass, the second moment is shown to depend on width of the field distribution and not the mean. Calculations are in progress for model field distributions.

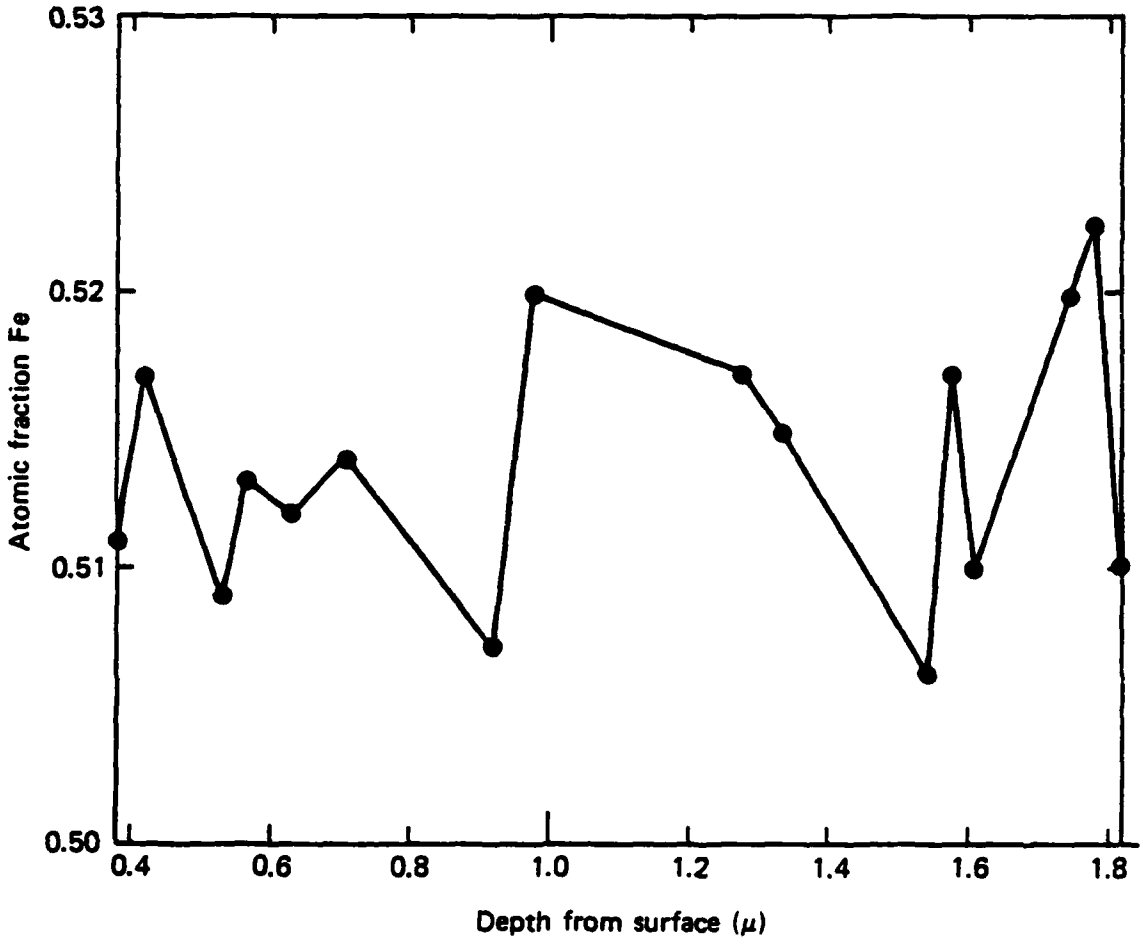

Fig. 1. Variations with depth in iron stoichiometry in a typical sputtered Fe-B film (#22 on glass); average atomic fraction of iron: 0.514±0.004.

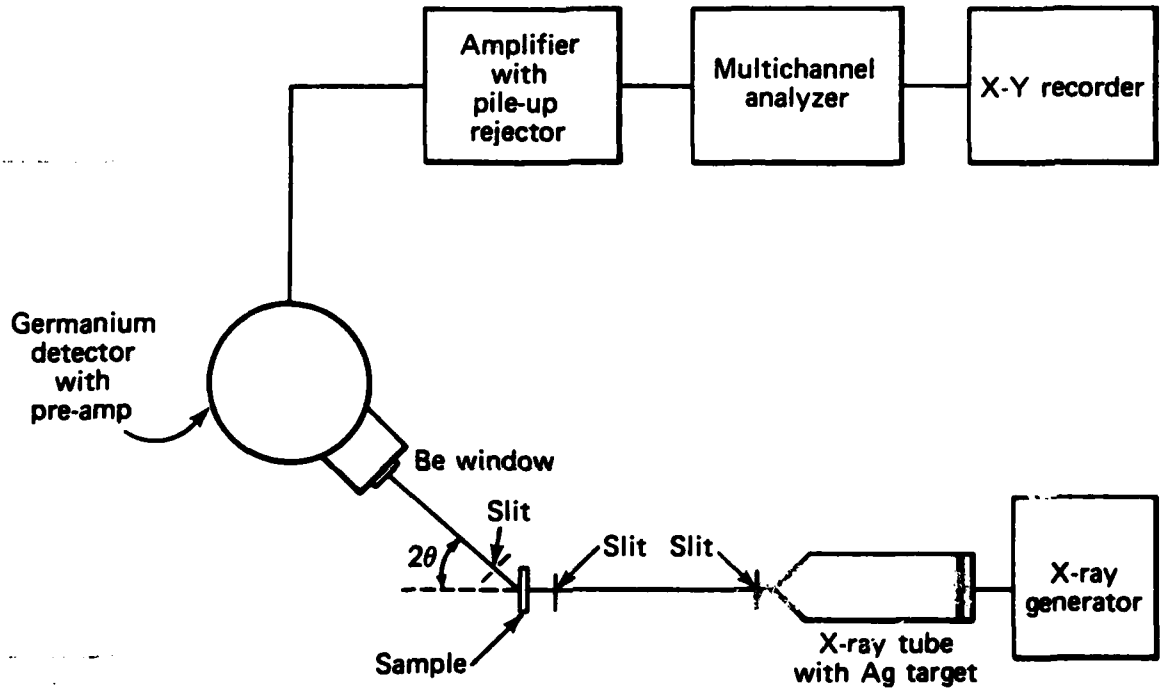

Fig. 2. Energy dispersive X-ray diffraction system.

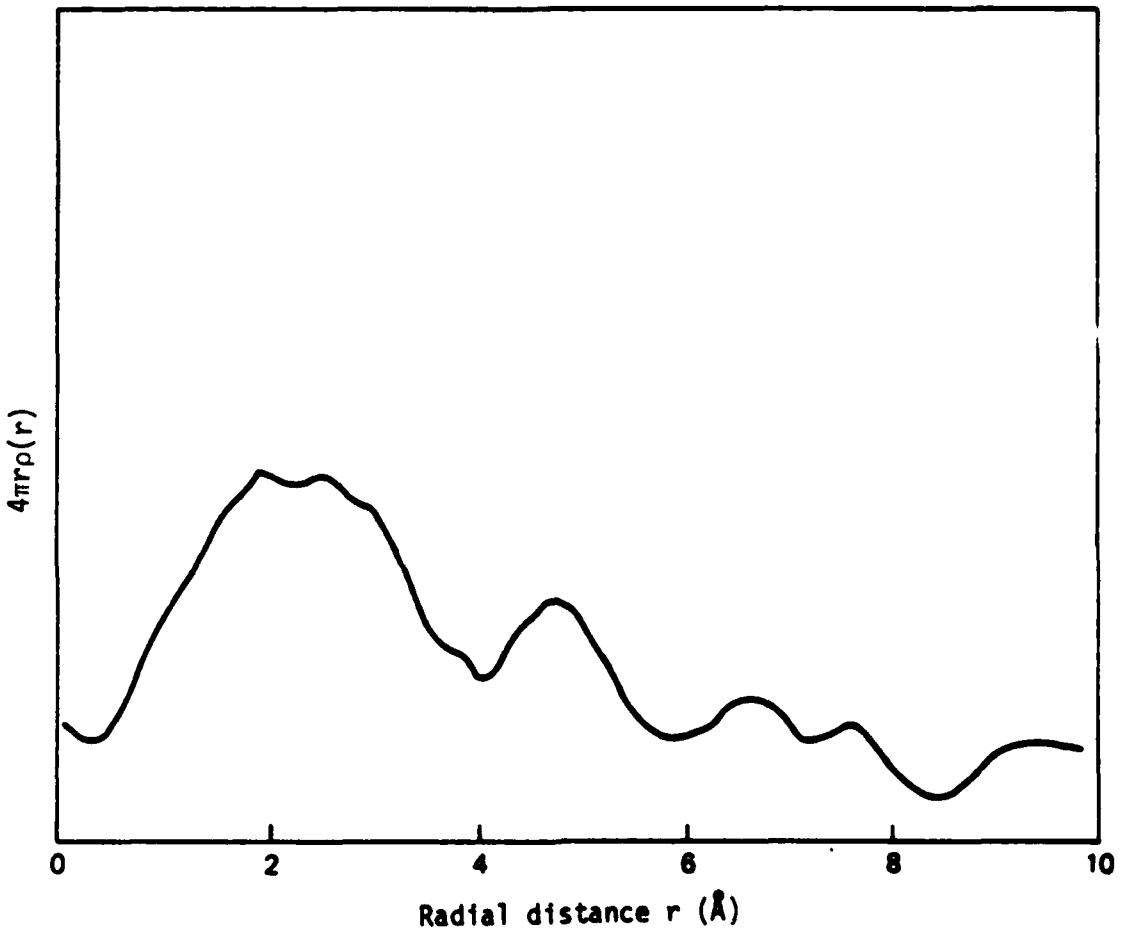

Fig. 3. Radial distribution function for a-$Fe_{71}B_{29}$.

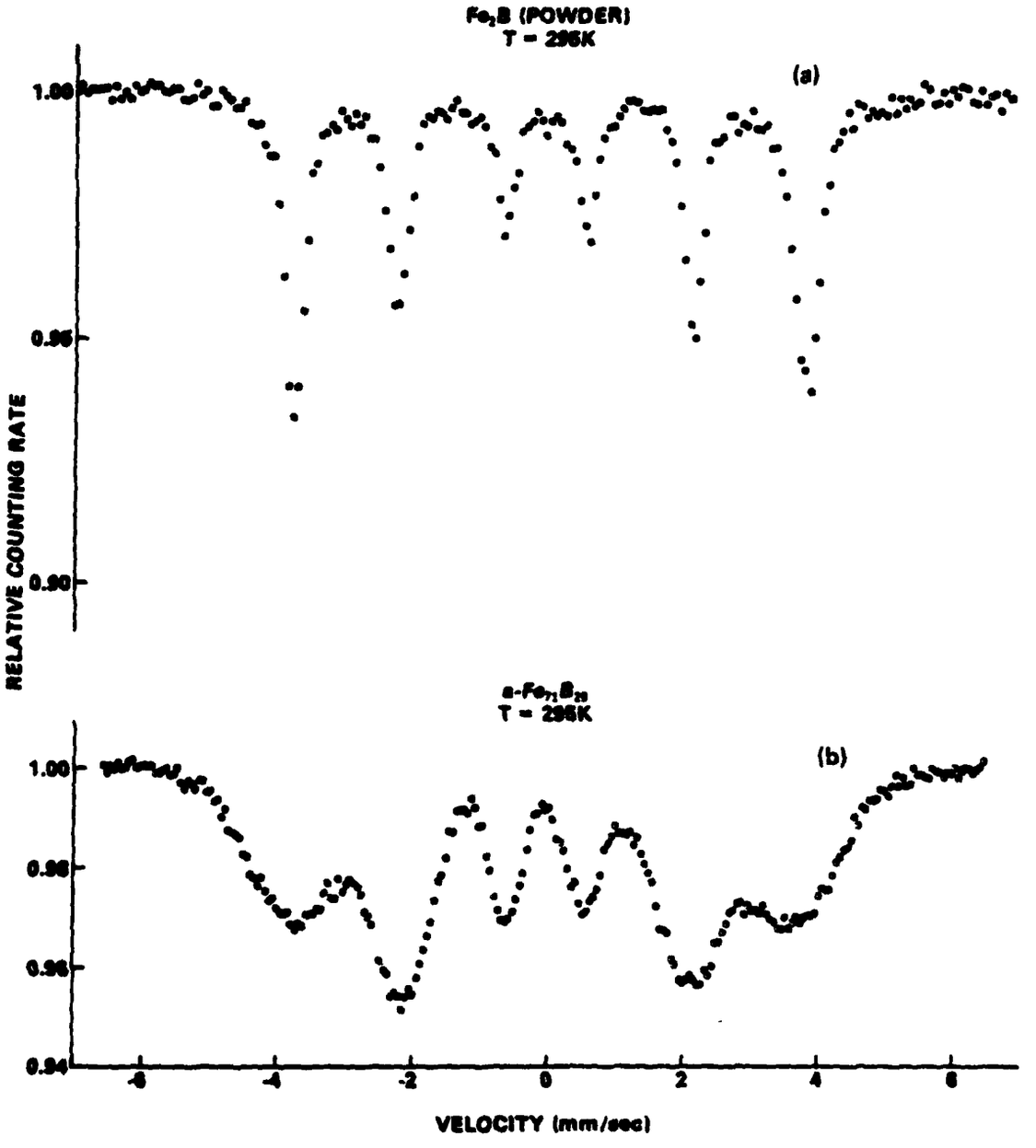

Fig. 4. (a) Spectrum of Fe_2B (powder) compared with (b) spectrum of a-$Fe_{71}B_{29}$ sputtered film.

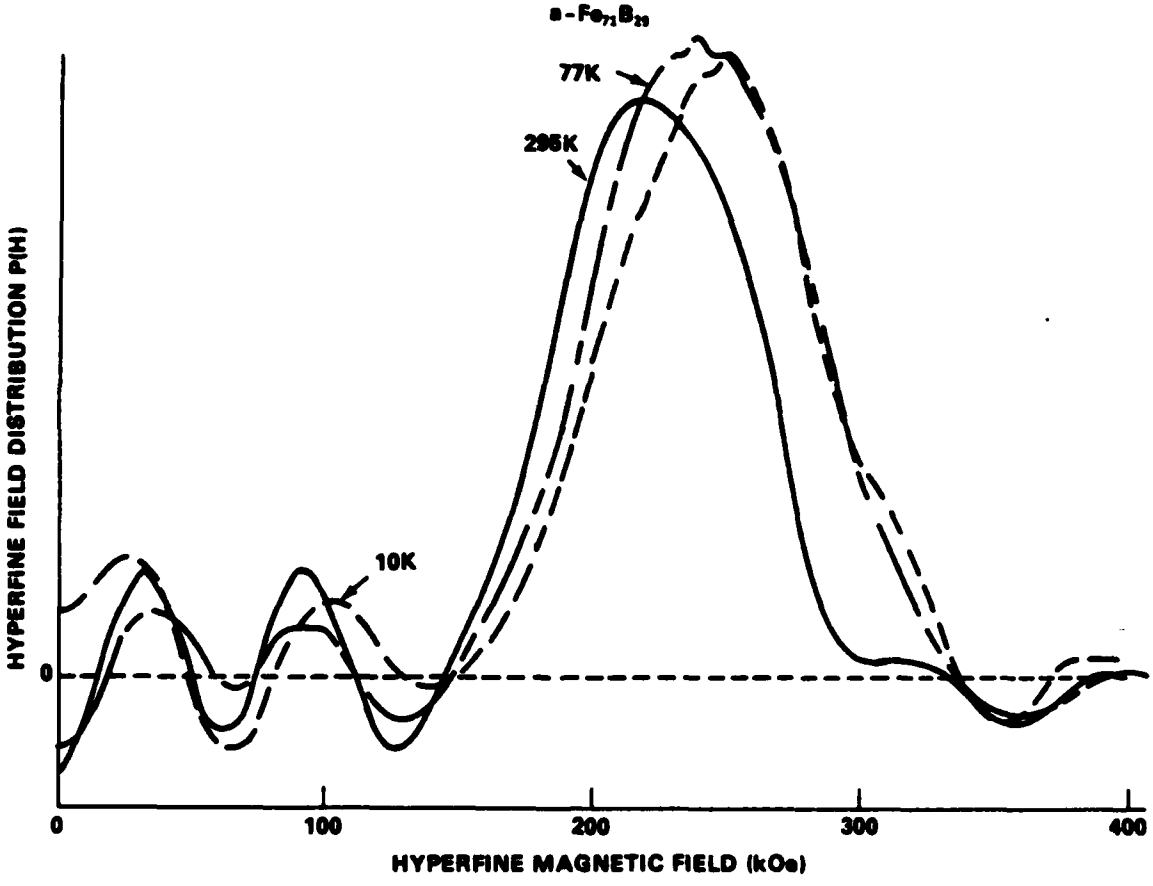

Fig. 5. P(H) distributions for a-$Fe_{71}B_{29}$ at 295, 77, and 10 K.

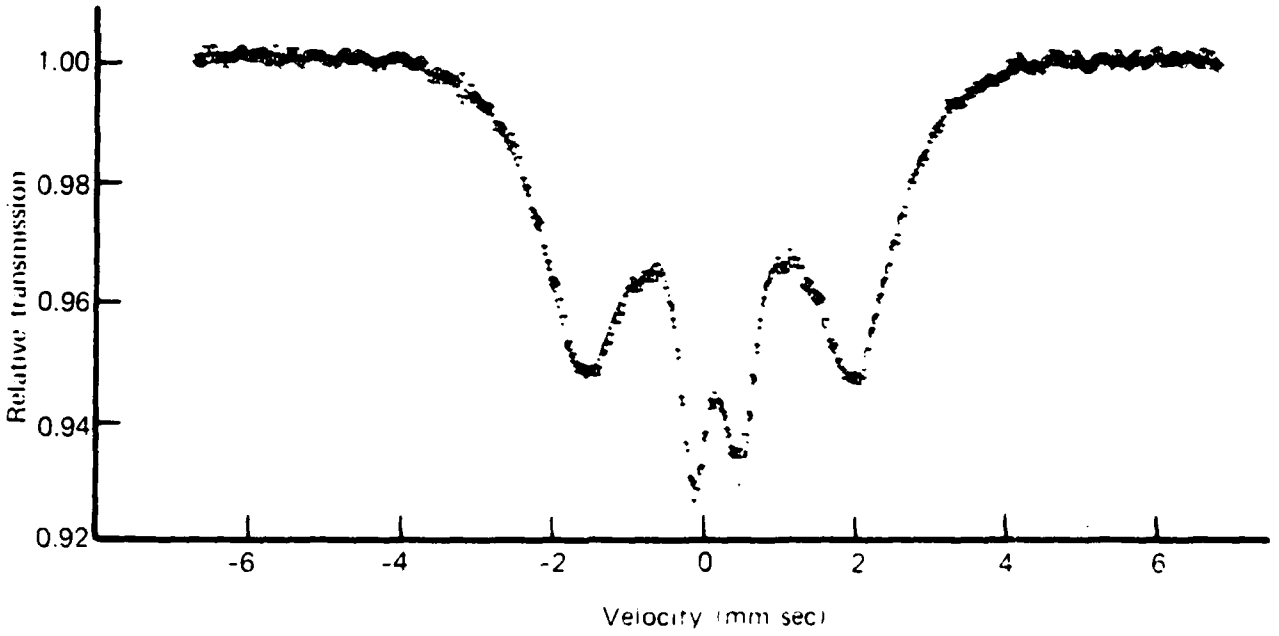

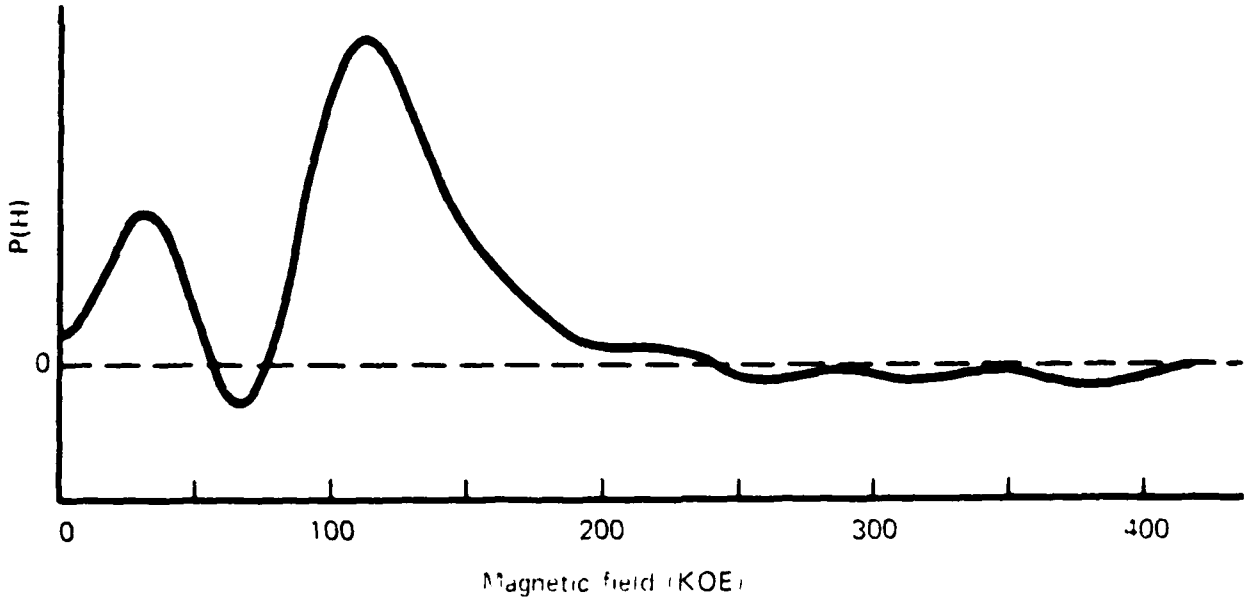

Fig. 6. Mössbauer spectrum and least squares optimized magnetic hyper fine field distributions P(H) for sputtered amorphous $Fe_{53}B_{47}$ film at T = 295 K.

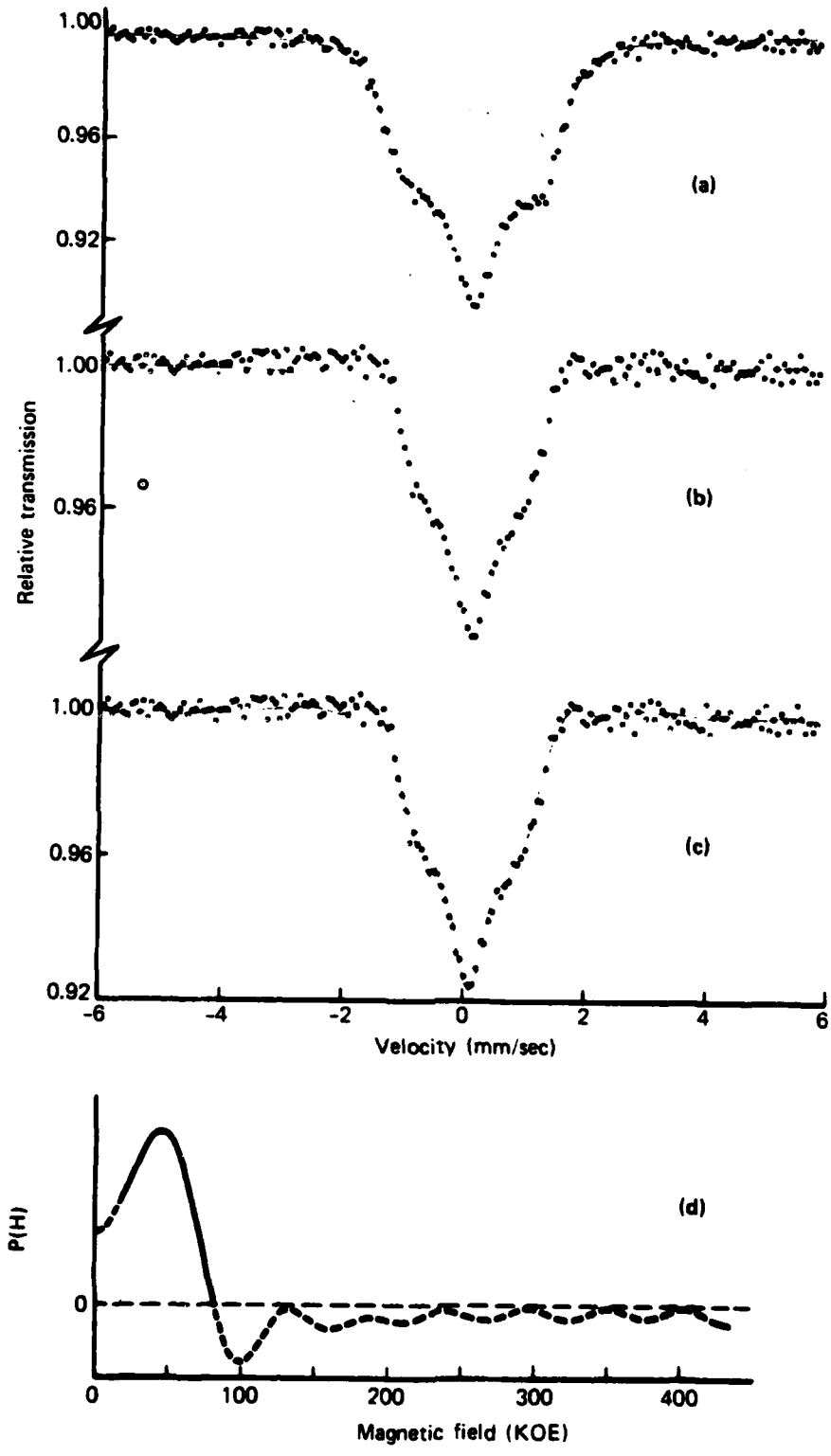

Fig. 7. (a) Spectrum of a-$Fe_{40}B_{60}$: H_{app} = 80 kOe, T = 4.2 K. Solid line is theoretical diagmagnetic components. (b) Same as (a) with theoretical spectrum subtracted ("stripped" data). (c) Stripped data with solid line showing spectrum from P(H) fit. (d) P(H) giving best fit to stripped spectrum. Dashed line represents meaningless part of distribution.

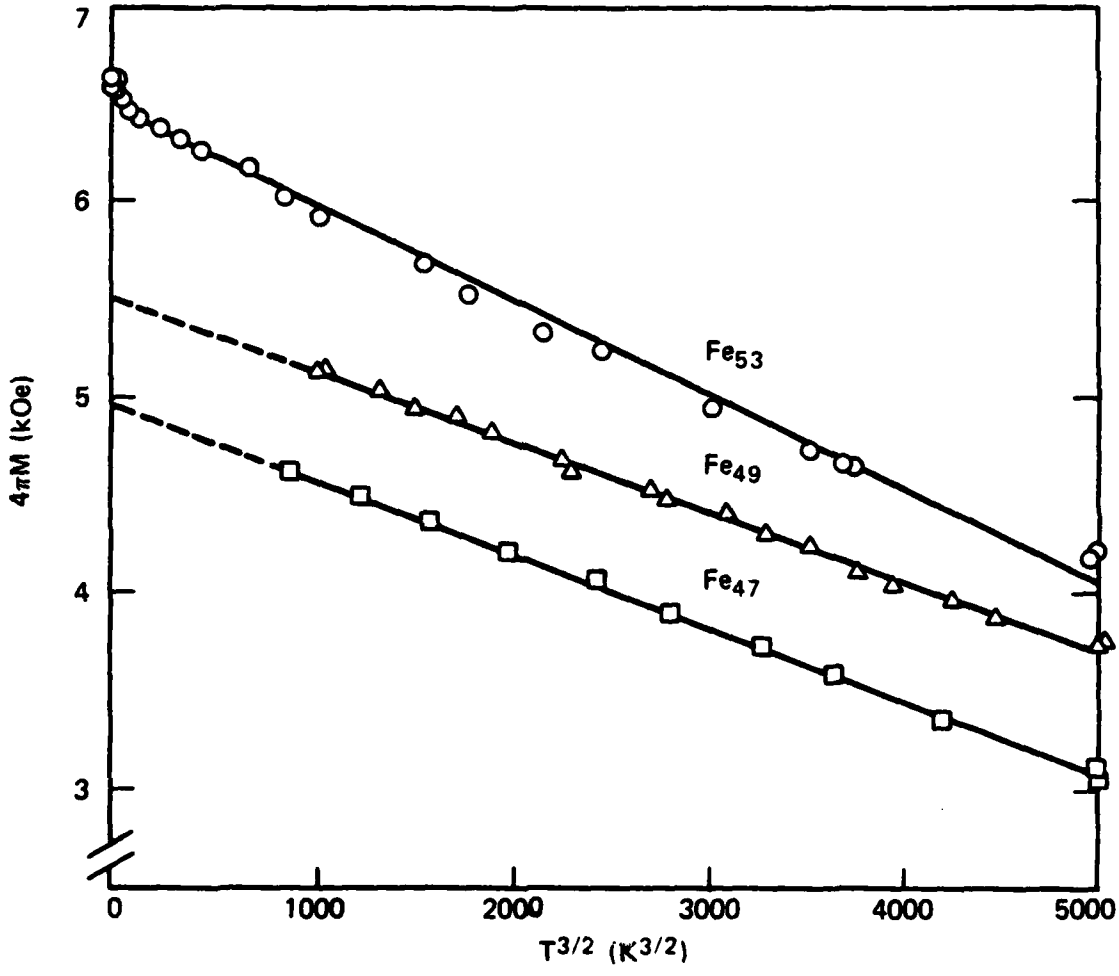

Fig. 8. Temperature dependence of the magnetization deduced from FMR data on amorphous Fe_xB_{1-x} alloys. As described in the text, below 80 K, Fe_{47} and Fe_{49} do not show simple behavior, hence the dashed lines.

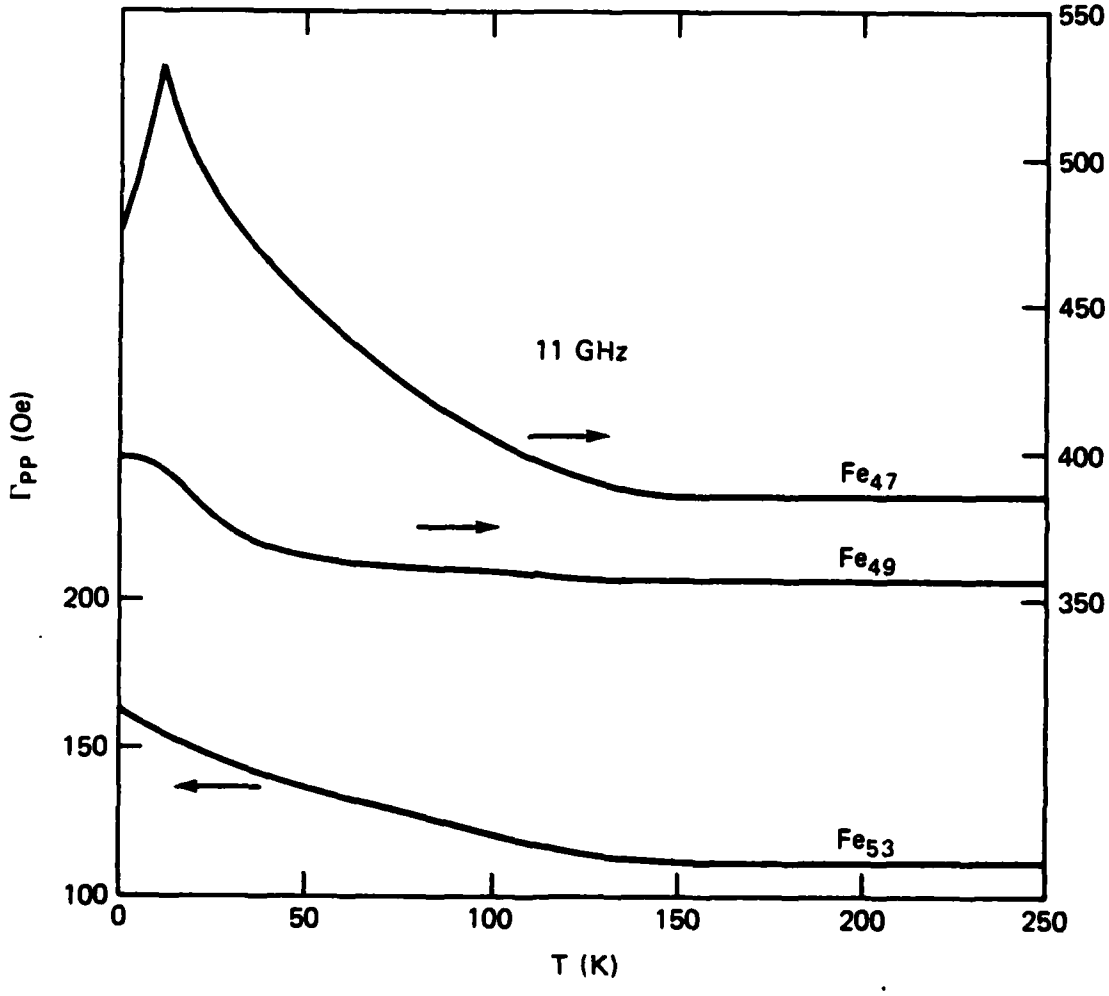

Fig. 9. Temperature dependence of the FMR linewidths at 11 GHz for amorphous Fe_xB_{1-x} alloys.

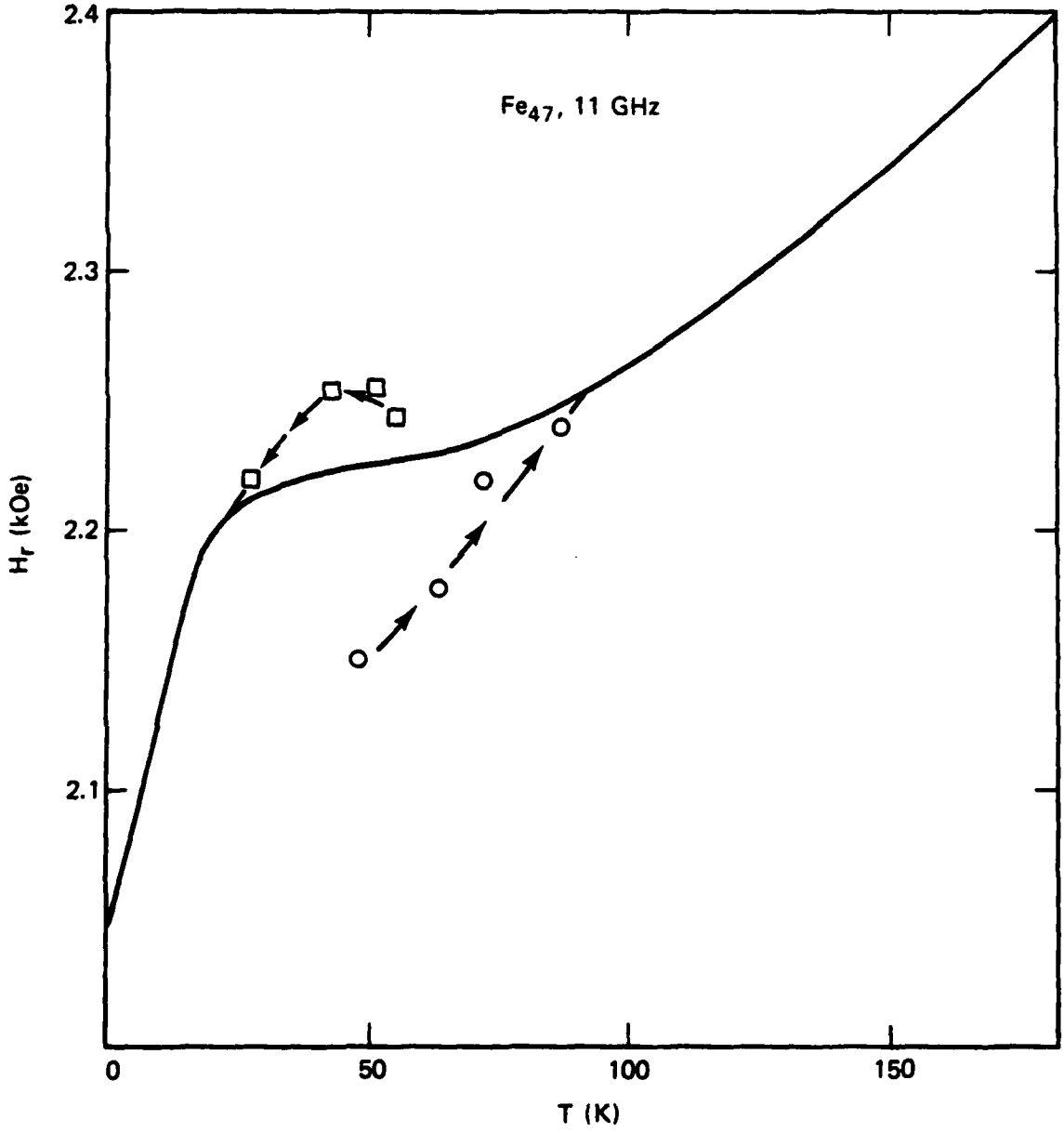

Fig. 10. Temperature dependence of the resonance field for FMR in amorphous Fe_{47}. Below 80 K, the data are dependent upon the thermal history. The solid line is obtained on slow (~0.25 K/min) cooling while the other data represent other thermal cycles.

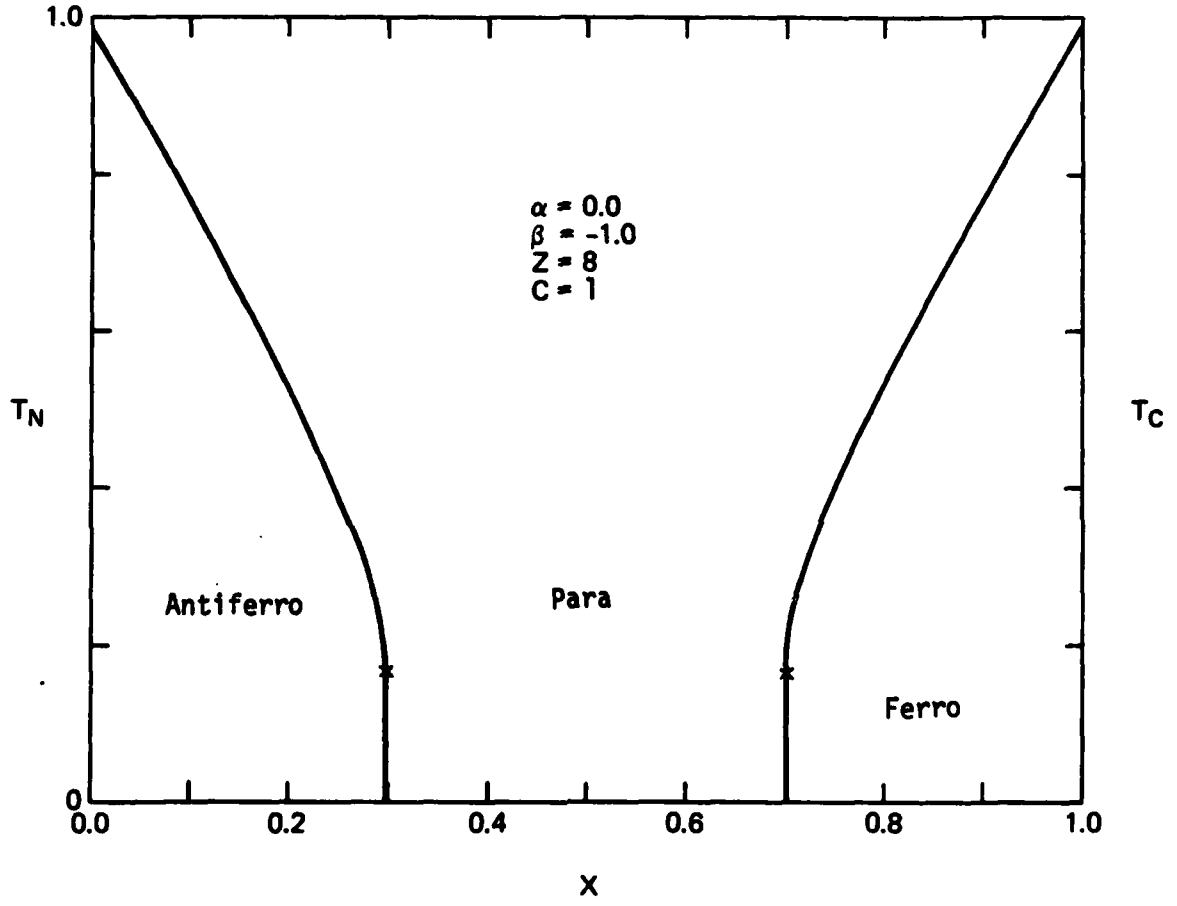

Fig. 11. Magnetic phase diagram for the alloy $(A_xB_{1-x})_cD_{1-x}$; T_C and T_N are normalized Curie and Néel temperatures. For definition of other parameters, see text.

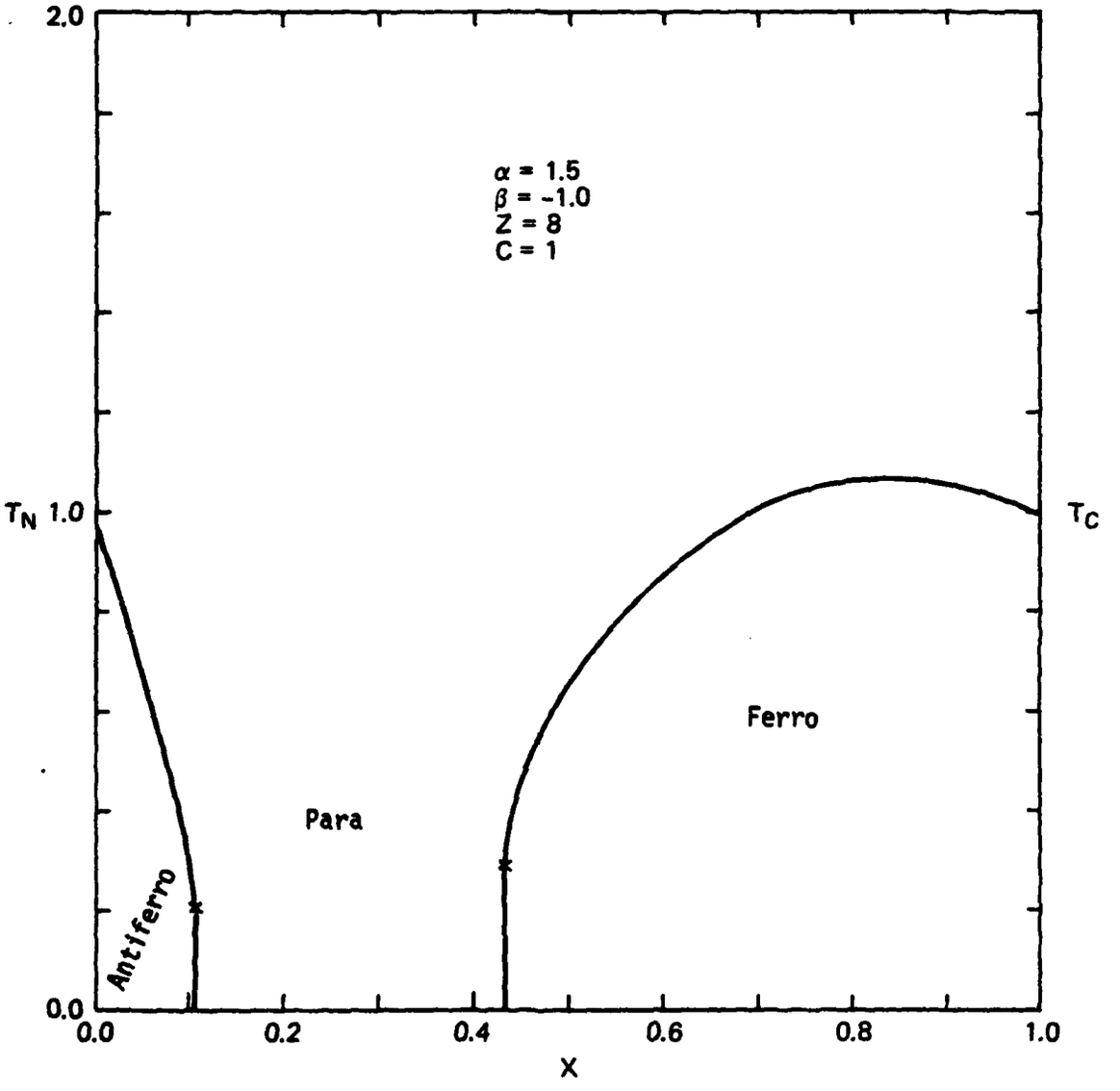

Fig. 12. Magnetic phase diagram for the alloy $(A_xB_{1-x})_cD_{1-c}$; T_C and T_N are normalized Curie and Néel temperatures. For definition of other parameters, see text.

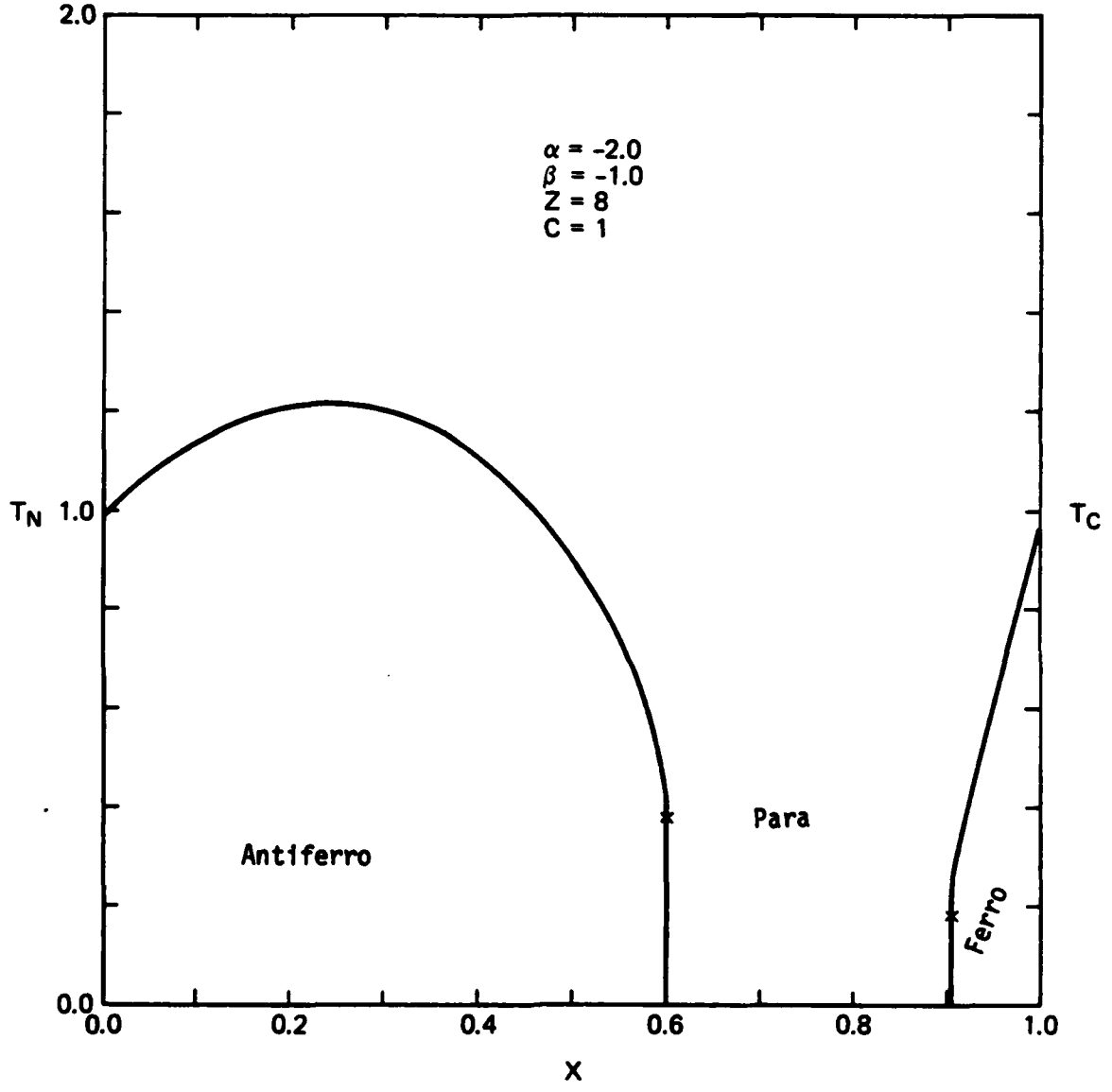

Fig. 13. Magnetic phase diagram for the alloy $(A_xB_{1-x})_cD_{1-c}$; TC and TN are normalized Curie and Néel temperatures. For definition of other parameters, see text.

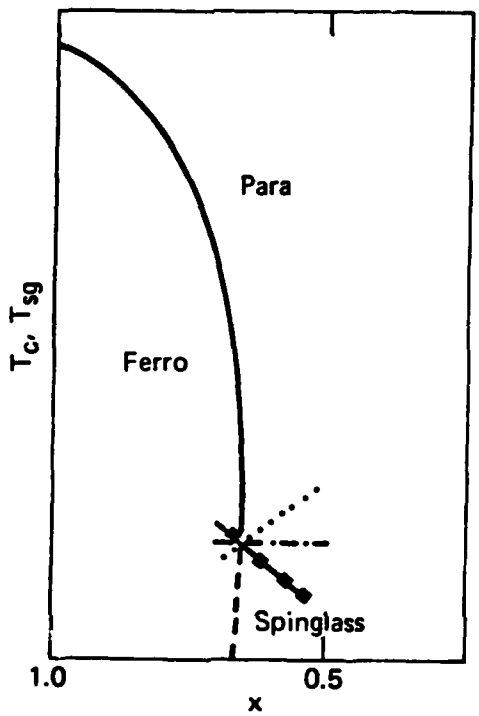

Fig. 14. Magnetic phase diagram (schematically) for the model discussed in the text. The three para-spinglass phase boundaries correspond to the greater than (····), equal to (-·-·-·) and less than (■-■-■-) signs in Eq. (7).

Table I. Isomer shifts (δ), magnetic ordering temperature (T_c) and value of H for which P(H) is maximum (H_{peak}) for several amorphous alloys, polycrystalline Fe_2B and the metastable phase Fe_3B. Isomer shifts are relative to α-Fe with source and absorber at 300 K.

Sample	δ(mm/sec)	T_c(K)	H_{pk}(kOe)
a-$Fe_{71}B_{29}$ (sputtered)	+0.12	$\gtrsim$750	222
a-$Fe_{72}B_{28}$ (melt-quenched)	+0.09	760	245
a-$Fe_{80}B_{20}$ (Metglas alloy)	+0.07	685	255
Fe_2B (polycrystalline powder)	+0.12	1015	236
Fe_3 (metastable)	+0.5 to +0.14	~820	242 to 305 (at least 3 distinct magnetic sites)

II. Summary of Important Results

In our studies on a-Fe_xB_{100-x} alloys, we have produced sputtered films of the alloys that are chemically and magnetically homogeneous. This has required a proper choice of source materials and holders and a careful control over deposition parameters. The excellent results could not have been achieved without the examination of the samples by SIMS and ferromagnetic resonance and incorporating the findings in refinement of the sputtering equipment. It should be emphasized that chemical and magnetic homogeneity is essential to controllable tailored materials and applications in magnetic devices.

Mössbauer studies, besides yielding relevant magnetic parameters for the alloys, have thrown light on the structure of the alloys. Though the chemical short range order in metallic glasses has been demonstrated to be similar to that in corresponding crystalline alloys, our results indicate this to be true only for iron concentration, x, larger than ~0.7. For alloys with x in the vicinity of 0.5, the chemical short range order is significantly different from that in crystalline FeB for about 30 per cent of the Fe sites. Such alloys also possess a magnetic ground state (spin glass) that is different from the ferromagnetic state of the crystalline FeB. The understanding of the modification of chemical and magnetic short range order would be extremely valuable for tailoring various properties of materials.

The experimental program has benefited from the guidance and interpretation provided by accompanying theoretical modeling. A model, pre-

viously designed for the study of evolution and behavior of ferromagnetism in disordered binary alloys, has been generalized to include ternary alloys and to consider the possibility of competing exchange interactions and the resulting spin glass phase. The trends predicted for the stability of various magnetic phases in disordered alloys have been experimentally observed in a number of amorphous magnetic alloys.

III. Publications

K. Moorjani, S. K. Ghatak, K. V. Rao, B. Kramer, and H. S. Chen, "Spin Glass - Paramagnetic Phase Boundary in Amorphous Magnetic Alloys," J. Phys. (Paris), Colloquia C8, C8-718 (1980).

N. A. Blum, K. Moorjani, T. O. Poehler, and F. G. Satkiewicz, "Hyperfine Field Distributions in Ferromagnetic Amorphous Fe_xB_{1-x} Thin Films," J. Appl. Phys. 52, 1808 (1981).

N. A. Blum, K. Moorjani, T. O. Poehler, and F. G. Satkiewicz, "Mössbauer Investigation of Sputtered Ferromagnetic Amorphous Fe_xB_{100-x} Films," J. Appl. Phys. 53, 2074 (1982).

D. J. Webb, S. M. Bhagat, K. Moorjani, T. O. Poehler, and F. G. Satkiewicz, "Spin Glass Behavior and Non-Ergodicity in Amorphous Iron-Boron Alloys," Solid State Comm. 43, 239 (1982).

N. A. Blum, "Mössbauer Study of Magnetism in an Amorphous $Fe_{40}B_{60}$ Sputtered Film," J. Appl. Phys. (to be published).

These publications are attached as Appendices 1-5.

IV. Participating Scientific Personnel

N. A. Blum - Co-Principal Investigator

P. Dunn

K. G. Hoggarth

J. W. Leight

K. Moorjani - Co-Principal Investigator

A. L. Rosasco*

F. G. Satkiewicz

W. W. Wise

*Received M. S. in Engineering from The Johns Hopkins University for her thesis entitled, "Characterization of Amorphous Iron Borides: The Radial Distribution Function."

V. References

1. T. Egami, Glassy Metals I, Eds. H.-J. Güntherodt and H. Beck, Springer-Verlag, Berlin, 1981, p. 25.

2. "Amorphous Iron Borides: Preparation, Structure, and Magnetic Properties," proposal submitted to U.S. Army Research Office by The Johns Hopkins University, Applied Physics Laboratory and Department of Mechanics and Materials Science, Enclosure 1 to AD-7092, May 1977, and references therein.

3. J. E. Jeffries and N. Hershkowitz, Phys. Lett. 30A, 187 (1969).

4. K. A. Murphy and N. Hershkowitz, Phys. Ref. B 7, 23 (1973).

5. B. Window, J. Phys. E 4, 401 (1971).

6. N. A. Blum, K. Moorjani, T. O. Poehler, and F. G. Satkiewicz, J. Appl. Phys. 53, 2074 (1982; attached as Appendix 3).

7. C. L. Chien, D. Musser, E. M. Gyorgy, R. C. Sherwood, H. A. Chen, F. E. Luborsky, and J. W. Walter, Phys. Rev. B 2, 283 (1979).

8. N. A. Blum, J. Appl. Phys. (1983), to be published (attached as Appendix 5).

9. N. A. Blum, K. Moorjani, T. O. Poehler, and F. G. Satkiewicz, J. Appl. Phys. 52, 1808 (1981; attached as Appendix 2).

10. I. Vincze, T. Kemeny, and S. Arajs, Phys. Rev. B 21, 937 (1980).

11. The program for generating mixed quadrupole/dipole Mössbauer spectra was developed in collaboration with A. N. Jette and is similar to the one described in: J. R. Gabriel and S. L. Ruby, Nucl. Instr. Meth. 36, 23 (1965).

12. D. J. Webb, S. M. Bhagat, K. Moorjani, T. O. Poehler, and F. G. Satkiewicz, "Spin Glass Behavior and Non-Ergodicity in Amorphous Iron-Boron Alloys," Solid State Comm. 43, 239 (1982, attached as Appendix 4).

13. P. W. Anderson, "Ill-Condensed Matter," Ed. R. Babian, R. Maynard, and G. Toulouse, North Holland (1978), p. 159; A. Blandin, J. Phys. (Paris), Colloquia 39, C6-1499 (1978).

14. K. Moorjani and S. K. Ghatak, J. Phys. C Solid St. 10, 1027 (1977).

15. H. Daver, O. Massenet, and B. K. Chakraverty in Amorphous Semiconductors, Eds. J. Stuke and W. Brenig, Taylor & Francis, Ltd., 1974, p. 1053.

16. An excellent survey of the work is included in Intl. Conf. on Magnetism, München, 1979, published in J. Mag. Magn. Mat., 15-18 (1980); also see F. E. Luborsky in Ferromagnetic Materials, Vol. 1, Ed. E. P. Wohlfarth, North Holland, 1980, p. 451.

17. Recent reviews are J. A. Mydosh and G. J. Nieuwenhys in Ferromagnetic Materials, Vol. 1, Ed. E. P. Wohlfarth, North Holland, 1980, p. 451; K. Binder in Ordering in Strongly Fluctuating Condensed Matter Systems, Ed. T. Riste, Plenum Press, 1979, p. 423.

18. S. F. Edwards and P. W. Anderson, J. Phys. F. Met. Phys. 5, 965 (1975).

19. S. K. Ghatak and K. Moorjani, J. Phys. C Solid St. 9, L293 (1976).

20. K. Moorjani and S. K. Ghatak (to be published).

21. K. Moorjani, S. K. Ghatak, K. V. Rao, B. Kramer, and H. S. Chen, "Spin Glass - Paramagnetic Phase Boundary in Amorphous Magnetic Alloys," J. Phys. (Paris), Colloquia C8, C8-718 (1980, attached as Appendix 1).

APPENDICES

APPENDIX 1

K. Moorjani, S. K. Ghatak, K. V. Rao, B. Kramer, and H. S. Chen, "Spin Glass - Paramagnetic Phase Boundary in Amorphous Magnetic Alloys," J. Phys. (Paris), Colloquia C8, C8-718 (1980).

APPENDIX 2

N. A. Blum, K. Moorjani, T. O. Poehler, and F. G. Satkiewicz, "Hyperfine Field Distributions in Ferromagnetic Amorphous Fe_xB_{1-x} Thin Films," J. Appl. Phys. 52, 1808 (1981).

APPENDIX 3

N. A. Blum, K. Moorjani, T. O. Poehler, and F. G. Satkiewicz, "Mössbauer Investigation of Sputtered Ferromagnetic Amorphous Fe_xB_{100-x} Films," J. Appl. Phys. 53, 2074 (1982).

APPENDIX 4

D. J. Webb, S. M. Bhagat, K. Moorjani, T. O. Poehler, and F. G. Satkiewicz, "Spin Glass Behavior and Non-Ergodicity in Amorphous Iron-Boron Alloys," Solid State Comm. 43, 239 (1982).

APPENDIX 5

N. A. Blum, "Mössbauer Study of Magnetism in an Amorphous $Fe_{40}B_{60}$ Sputtered Film," J. Appl. Phys. (to be published, 1983).

APPENDIX 1

JOURNAL DE PHYSIQUE — Colloque C3, Supplément au n°8, Tome 41, août 1980, page C3-718

SPIN GLASS - PARAMAGNETIC PHASE BOUNDARY IN AMORPHOUS MAGNETIC ALLOYS

K. Moorjani*, S.K. Ghatak**, K.V. Rao***†, B. Kramer***† and H.S. Chen×

*Johns Hopkins University, Applied Physics Laboratory Laurel, Maryland 20910, U.S.A.
**Physics Department, Indian Institute of Technology, Kharagpur, W. Bengal, India.
***Department of Physics, University of Illinois at Urbana-Champaign, Urbana, Illinois 61801, U.S.A.
×Bell Laboratories, Murray Hill, New Jersey 07975, U.S.A.

Abstract.- A compositionally disordered magnetic alloy $(A_xB_{1-x})_cD_{1-c}$ where A and B are magnetic species while D represents the nonmagnetic atoms is considered. The competition among the exchange interactions J_{AA}, J_{AB} and J_{BB} in these alloys can lead to the disappearance of the ferromagnetism (for ferromagnetic J_{AA}) below a critical concentration x_c. For $x < x_c$, we show that while the appearance of the spin glass state at low temperatures is dependent on the relative signs of the exchange interaction, the details of the phase boundaries are controlled by the relative strength of the exchange interactions. These conclusions are borne out by our experimental results on the amorphous metal-metalloid alloys $(Fe_xNi_{1-x})_{75}G_{25}$, $(Fe_xMn_{1-x})_{75}G_{25}$ and $(Co_xMn_{1-x})_{75}G_{25}$ where $G_{25} \equiv P_{14}B_6Al_3$. The magnetic phase diagrams for the three alloy systems were obtained from the ac susceptibility measurements and while the slope of the spinglass paramagnetic phase boundary in the vicinity of the tricritical point is negative for the Fe-Ni alloy, it is almost zero for the Fe-Mn alloy and is positive for the Co based alloy.

Introduction. Spin glass behavior has been observed in a large number of systems including dilute alloys, where magnetic impurities are distributed at random on a crystalline lattice; or concentrated alloys, which are compositionally and/or topologically disordered [1]. Both metallic and insulating solids have been shown to exhibit the spin glass state and it is well established that competing exchange interactions, when present in adequate proportion, are the essential element for the existence of such a state.

In a previous paper [2], we have obtained the magnetic phase diagram for a bond disordered alloy in which ferromagnetic and antiferromagnetic bonds are randomly distributed on a lattice with a probability distribution $P(J) = x\delta(J-J_1) + (1-x)\delta(J-J_2)$, where $J_1 > 0$, $J_2 < 0$ and x is the concentration of J_1 bonds while (1-x) that of J_2 bonds. For such a distribution, it was shown [2] that below a critical concentration x_c, the spin glass state results with a transition temperature, T_{sg}, proportional to $[xJ_1^2 + (1-x)J_2^2]^{\frac{1}{2}}$. Thus the spin glass-paramagnetic phase boundary, defined by dT_{sg}/dx, exhibits an initial slope which is positive, zero or negative depending on whether the magnitude of J_1 is greater than, equal to or less than the magnitude of J_2. The zero slope case results from the fact that for $J_1 = |J_2|$, T_{sg} is independent of x. The situation is equivalent to the case of symmetric continuous distribution of J (e.g. Gaussian distribution) which also leads to a phase boundary with zero slope [3].

In the present investigation we analyze the random site disordered model and show the validity of the general conclusions regarding the phase boundary briefly described above for the bond case. Certain modifications that result for the site case and the relevance of the conclusions to our experimental data on amorphous metal-metalloid alloys is described below.

*Supported in part by U.S. Army Research Office and by Naval Sea Systems Command, Contract N00024-78-C-5384.
†Supported by NSF-MRL Grant No. 77-23999.

Model. A compositionally disordered random magnetic alloy $(A_xB_{1-x})_cG_{1-c}$ is considered where A and B are magnetic species while G represents non-magnetic atoms. The exchange interaction J_{AA} is taken to be positive so that the pure A system (x=1, c=1) is ferromagnetic below a certain critical temperature T_c. The system remains ferromagnetic with reduced values of T_c, for values of c in the range $c_0 \leq c < 1$ where c_0 is the critical concentration for the onset of ferromagnetism in the alloy A_cG_{1-c}. For $c \geq c_0$, we investigate the disappearance of ferromagnetism in the alloy $(A_xB_{1-x})_cG_{1-c}$ as interactions J_{AB} and J_{BB} are introduced where at least one of them is antiferromagnetic. It is shown that for $x < x_0$, depending on the temperature, ferromagnetism disappears into a paramagnetic or a spin glass state. Of particular interest in the present study is the phase boundary between these two states which is found to be determined by the relative strength of J_{AB} and J_{BB} with respect to J_{AA}. In particular T_{sg} is found to increase, decrease or stay constant with decreasing x depending on the relative strengths of the exchange constants. The confirmation of these trends is found in our experimental results on amorphous metal-metalloid alloys with c = 0.75 and A = Fe or Co while B = Ni or Mn, and $G_{.25} = P_{.16}B_{.06}Al_{.03}$. The magnetic phase diagrams for these alloys are obtained from ac susceptibility measurements and it is found that in vicinity of the tricritical point, T_{sg} increases with decreasing x for $(Co_xMn_{1-x})_{.75}G_{.25}$ while it decreases in $(Fe_xNi_{1-x})_{.75}G_{.25}$ and is essentially constant for $(Fe_xMn_{1-x})_{.75}G_{.25}$.

Analysis. The random alloy $(A_xB_{1-x})_cG_{1-c}$ is represented by a Heisenberg Hamiltonian which is analyzed within the Bethe-Peierls-Weiss approximation. The details of the methodology have been previously described for amorphous binary alloys [4], spin glasses with Gaussian distribution of exchange interactions [5] and bond disordered random magnet [2], and will not be repeated here. It is sufficient to state that in BPW approximation, one considers a cluster of a central spin S_0 and its z nearest neighbors S_Δ s embedded in an effective medium defined by an internal field (H_i-H_e) which acts on the atoms on the surface of the cluster; H_e being the externally applied field. The Hamiltonian is then written as

$$\mathcal{H} = -\sum_{\Delta} J_{0\Delta}\vec{S}_0\cdot\vec{S}_\Delta - \vec{H}_e\cdot\vec{S}_0 - \vec{H}_i\cdot\sum_{\Delta}\vec{S}_\Delta \qquad (1)$$

where $J_{0\Delta} = J$ is a variable which for our random alloy takes on values according to the probability distribution

$$P(J) = x^2c^2\delta(J-J_{AA}) + (1-x)^2c^2\,(J-J_{BB}] + 2x(1-x)c^2\delta(J-J_{AB}] + (1-c^2)\delta(J]. \qquad (2)$$

The partition function Z for the above Hamiltonian is most easily calculated in the limit of large z, where it can be obtained in a form that facilitates [2, 4] taking the configurational average of the free energy (i.e. ln Z). Taking the Edwards-Anderson order parameter for the spin glass state [6], we find that the phase boundaries are defined by the equations [2],

$$2\langle\tilde{J}^2\rangle + 2zQ\langle\tilde{J}\rangle + 3 = 0 \text{ Ferro-Para} \qquad (3)$$

and

$$\langle\tilde{J}^2\rangle = \frac{1}{2}\,(2z^2Q^2-3) \text{ Para-Spin glass} \qquad (4)$$

where,

$$\tilde{J} = \frac{JS}{2k_iQ} = aJ \text{ and } Q = \left[\frac{2}{3}\,zS^2\right]^{-\frac{1}{2}}. \qquad (5)$$

The angular brackets in Eqs. (3) and (4) represent the configurational average over the probability distribution [Eq. (2)], which is readily performed to obtain,

$$\langle\tilde{J}\rangle = ac^2J_{AA}^2[x^2 + (1-x)^2\Sigma + 2x(1-x)\alpha] \qquad (6)$$

and

$$\langle \tilde{J}^2 \rangle = z^2 c^2 J_{AA}^2 [x^2 + (1-x)^2\beta^2 + 2x(1-x)\alpha^2] \quad (7)$$

where $\alpha = J_{AB}/J_{AA}$ and $\beta = J_{BB}/J_{AA}$. These equations are used to obtain complete phase diagrams and details of the calculation, without the large z restriction, will be published elsewhere [7]. Here our main concern is the spin glass-paramagnetic phase boundary and this is obtained by substituting Eq. (7) in Eq. (4) to obtain (S=1)

$$\left(\frac{kT_{sg}}{zJ_{AA}}\right)^2 = \frac{1}{36}\frac{z}{z-1} c^2[x^2 + 2x(1-x)\alpha^2 + (1-x)^2\beta^2]. \quad (8)$$

Therefore the sign of dT_{sg}/dx is determined by the expression $[x + (1-2x)\alpha^2 - (1-x)\beta^2]$. Thus, in the vicinity of the tricritical point x_t, $dT_{sg}/dx|_{x_t}$ is positive, zero or negative depending on whether

$$|\beta| \lessgtr \left[\frac{x_t + (1-2x_t)\alpha^2}{(1-x_t)}\right]^{\frac{1}{2}} \quad (9)$$

Schematic phase diagram based on above considerations is shown in Figure 1.

Experiment. All the alloys in the three systems, Co-Mn, Fe-Mn and Fe-Ni, were prepared in the form of ribbons by the melt spinning technique on the outer surface of a rotating copper-bronze disc [8]. X-ray techniques were used to ascertain the amorphous nature of the alloys. Low field ac-susceptibility techniques were used to determine the magnetic ordering temperatures in both the ferromagnetic and spin glass regimes of the alloys.

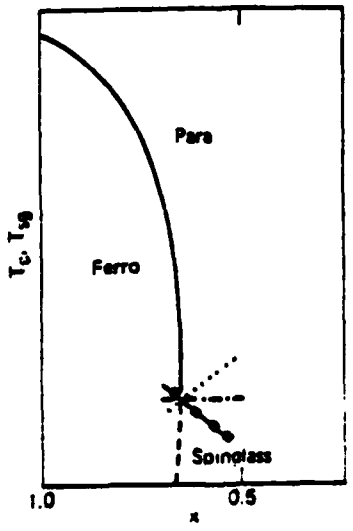

Figure 1.

Phase diagram (schematically) for the model discussed in the text. The three para-spin glass phase boundaries correspond to greater than (···), equal to (-·-·-·) and less than (▪-▪-▪-)signs in Eq. (9).

About 3 mm lengths were cut from ribbons of amorphous alloys of approximately 1.55 mm×(25–40) μm cross-section and packed to form a cylinder embedded in candle wax. This was then packed in the coil of an ac-susceptibility bridge [9] with the longer dimension along the coil axis. The ac-susceptibility was measured in a field of ∿ 3 Oe (rms) at 300 Hz. A check at several frequencies between 100 Hz and 1 Khz showed no significant differences in the data obtained. Data taken both on warming and cooling the sample were completely reproducible. The absolute temperature of the sample, in good thermal contact through an He exchange gas with the cooling/warming chamber, was determined using a calibrated platinum thermometer. In the ferromagnetic regime, the ac-susceptibility as a function of temperature exhibited a sharp rise near T_C, and achived a constant value, determined by the appropriate demagnetization factor, below it. The temperature corresponding to the 'kink-point' was then taken as the Curie temperature T_C. The values of T_C thus obtained agree to within ±2K with those determined by other standard techniques like, for example, VSM measurements. At concentrations corresponding to the spin glass regime, a sharp characteristic ac-susceptibility cusp was observed for all the alloys and the spin glass temperature, T_{sg}, was thus determined to better than ±1K.

Results. In the Fe-Mn alloys, Fe and Mn possess comparable moments and while nearest neighbor Fe-Fe pairs are ferromagnetically coupled, the nearest

neighbor Mn-Mn and Fe-Mn pairs are antiferromagnetically coupled. Figure 2 depicts the observed

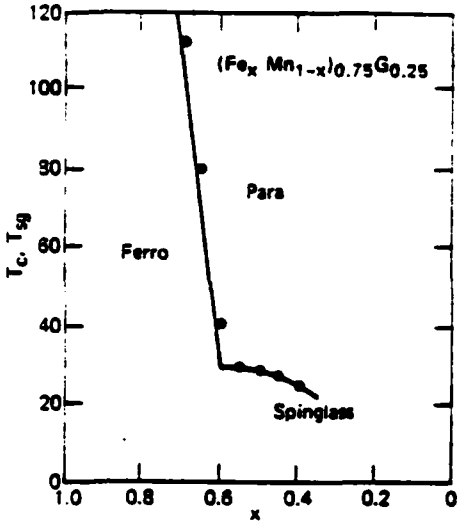

Figure 2

Phase diagrams for the amorphous alloy series $(Fe_xMn_{1-x})_{0.75}P_{0.12}B_{0.06}Al_{0.03}$.

transition temperatures as a function of the alloy composition for the amorphous $(Fe_xMn_{1-x})_{.75}G_{.25}$ series. Ferromagnetism prevails for $x \geq 0.6$ and increasing concentration of Mn introduces enough competition among exchange interactions (frustration) to lead to the spin glass phase. It has been shown that the magnetic susceptibility along the spin glass-paramagnetic phase boundary as well as the ferromagnetic-paramagnetic boundary of this series of alloys satisfies a scaling hypothesis appropriate to a multicritical point common to both boundaries [10]. The value of T_{sg} and the magnitude of the susceptibility at T_{sg}, both decrease with decreasing value of x from 0.6 to 0.4. The initial drop in T_{sg} near the multicritical point is however very slow and the slope of the paramagnetic-spin glass phase boundary is almost zero corresponding to the equality sign in Eq. (9).

Figure 3 shows the concentration dependence

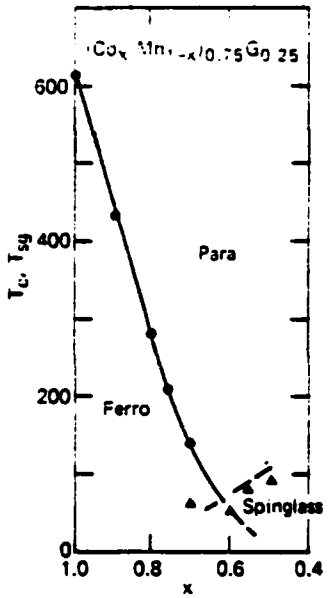

Figure 3.

Phase diagram for the amorphous alloy series $(Co_xMn_{1-x})_{0.75}P_{0.12}B_{0.06}Al_{0.03}$.

of the transition temperatures (T_c, T_{sg}) for the alloy series $(Co_xMn_{1-x})_{.75}G_{.25}$. Again, while this alloy is a ferromagnet for $x > 0.75$, a spin glass type behavior is observed for $x < 0.6$. However, in contrast to the behavior observed in the case of Fe-Mn alloys, T_{sg} increases with higher concentrations of Mn for this system; a behavior predicted by the upper sign in Eq. (9). In addition, it is found that the maximum value of the susceptibility of T_{sg} decreases rather rapidly with further addition of Mn in this alloy system; so much so that it was not possible to obtain reliable T_{sg} values for $x < 0.4$ by this method. It is useful to point out that such an unusual behavior of the concentration dependence of T_{sg} has also been reported recently for crystalline Co-Mn alloys [11]. A further evidence for the observed slope of the spin glass-paramagnetic boundary is obtained from the ac-susceptibility data for alloy compositions close to the multicritical point. For example, it is found that for $x = 0.7$ alloy the ac-susceptibility exhibits a sharp characteristic kink-point correspond-

ing to the ferromagnetic transition, T_C = 110K, which is then followed by a sharp drop in χ_{ac} characteristic of a spin glass phase at a lower temperature T_{sg} ≈ 60K. Further details of these will be published elsewhere [12]. These lower transitions observed for alloy concentrations close to the multicritical point extrapolates well to the spin glass line as shown in Figure 3.

While the two amorphous alloy series described above belong to the concentrated spin glass systems, the series $(Fe_xNi_{1-x})_{.75}G_{.25}$ belongs to a dilute spin glass sytem. For the particular composition of the glass former chosen, Ni has essentially zero moment and simply acts as a diluant. The behavior in the spin glass region is indeed found to be similar to the dilute crystalline Au-Fe series [13]. As shown in Figure 4, the spin glass state sets in only for $x \leq 0.18$ and corresponding to the lower sign in Eq. (9), the value of T_{sg} decreases with decreasing x.

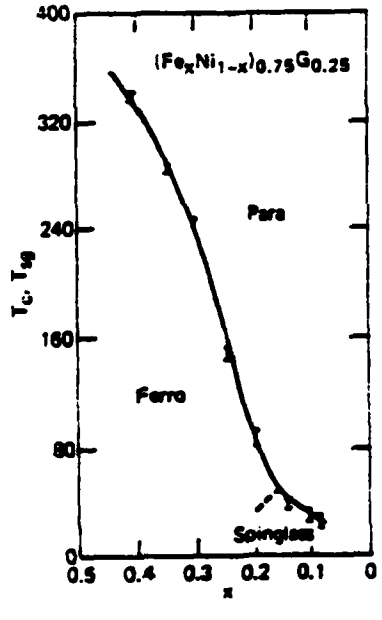

Figure 4

Phase diagram for the amorphous alloy series $(Fe_xNi_{1-x})_{0.75}P_{0.16}B_{0.06}Al_{0.03}$.

References

[1] Recent reviews on the subject include, A. Blandin, J. Physique, Colloq. 39 (1978) C6-1499; J. Soultie, J. Physique, Colloq. 39 (1978) C2-3; C. N. Guy, J. L. Tholence, H. Maletta, D. J. Thouless, J. A. Hertz, and S. Kirkpatrick, Panel Discussion: Spin Glasses, J. Appl. Phys. 50 (1979) 7308.

[2] K. Moorjani and S. K. Ghatak, Solid State Commun. 26 (1978) 357.

[3] D. Sherrington and S. Kirkpatrick, Phys. Rev. Lett. 35 (1975) 1792.

[4] K. Moorjani and S. K. Ghatak, J. Phys. C Solid St. 10 (1977) 1027.

[5] S. K. Ghatak and K. Moorjani, J. Phys. C Solid St. 9 (1976) L293.

[6] S. F. Edwards and P. W. Anderson, J. Phys. F Met. Phys. 5 (1975) 965.

[7] S. K. Ghatak and K. Moorjani (to be published).

[8] H. S. Chen and C. E. Miller, Mat. Res. Bull. 11 (1976) 49.

[9] R. W. Tustison (1976) Ph.D. Thesis, University of Illinois at Urbana-Champaign.

[10] M. B. Salamon, K. V. Rao, and H. S. Chen, Phys. Rev. Lett. 44 (1980) 596.

[11] D. R. Rhiger, D. Muller, and P. A. Beck, Proc. ICM79, Munich (1979) (to be published).

[12] K. V. Rao, B. Kramer, Y. Yesheran, and M. B. Salamon (to be published).

[13] B. R. Coles, B. V. B. Sarkissian, and R. H. Taylor, Phil. Mag. 937 (1978) 489.

Hyperfine field distributions in ferromagnetic amorphous Fe_xB_{1-x} thin films[a]

N. A. Blum, K. Moorjani, T. O. Poehler, and F. G. Satkiewicz

The Johns Hopkins University, Applied Physics Laboratory, Laurel, Maryland 20810

Sputtered films of amorphous Fe_xB_{1-x} ($0.40 \leq x \leq 0.50$) were studied by Mössbauer spectroscopy. The films were characterized for composition and homogeneity by secondary-ion mass spectrometry (SIMS) and for lack of crystallinity by X-ray diffraction. Below the magnetic ordering temperature T_c, the hyperfine spectra consist of a large amplitude quadrupole doublet superimposed on a broad magnetic hyperfine field distribution. The spectra of these alloys are remarkably different from that of polycrystalline FeB and from those of liquid-quenched alloys which are restricted to compositions near the eutectic at $x \simeq 0.8$. Comparison with the polycrystalline FeB spectrum clearly shows that for a significant fraction of the Fe atoms in the amorphous alloys, the local environment is substantially different from the Fe environment in FeB.

PACS numbers: 76.80. + y, 75.50.Kj, 75.50.Bb, 75.70.Dp

INTRODUCTION

Liquid-quenched $Fe_x B_{1-x}$ ($.72 \lesssim x \lesssim .86$) alloys can be prepared in an amorphous form which is stable at temperatures below about 400°C. These alloys are ferromagnetic with magnetic ordering temperatures T_c increasing from 279°C to 487°C with decreasing Fe concentration (1). At temperatures well below T_c the Mossbauer spectra are all similar to that of $Fe_{.80}B_{.20}$ and exhibit a well defined, though broadened, six-line magnetic hyperfine structure which can be understood as arising from a distribution of hyperfine fields P(H) due to the multitude of inequivalent Fe sites (2-4). Assuming a continuous distribution for P(H), it has been shown that for all of the above mentioned alloys P(H) may be described as a nearly symmetric, smooth peak of half-width about 100kOe, centered between about 270 and 310 kOe for x between .72 and .86 (1). In all cases there is no evidence that, below T_c, any appreciable fraction of the Fe atoms experiences a magnetic hyperfine field of zero. Similar results were obtained for amorphous $Fe_{.80}B_{.20}$ by assuming a discrete distribution $P(H_i)$, where five values of H_i were used, corresponding to the five most probable Fe near-neighbor configurations derived from the Bernal model of dense random packing (3).

We have carried out Mössbauer measurements on sputtered films of amorphous $Fe_x B_{1-x}$ in the concentration range $0.40 \leq x \leq 0.50$, quite different from the range usually available in liquid-quenched alloys. Our investigation shows that even below T_c, a substantial fraction of the Fe atoms experiences a very small, or zero magnetic hyperfine field. Furthermore, the values of electric quadrupole splitting for these alloys are found to be significantly different from that of the intermetallic crystalline compound FeB. These results indicate that the local surroundings of some of the Fe sites in these amorphous alloys are *different from the surroundings of Fe sites in the* corresponding crystalline compound; conclusion is in contrast to the reported behavior for x = 0.75 (5).

SAMPLE PREPARATION AND EXPERIMENTAL PROCEDURES

Films approximately 2 to 4 μm thick were sputtered in an argon atmosphere onto both beryllium foil and thin glass discs attached to a water-cooled heat sink maintained near room temperature. The source consisted of a mechanical mixture of FeB and boron powders contained in a shallow dish target holder fabricated entirely from soft iron. The composition of the source mix was varied from 32 to 40 at. % Fe to produce films with somewhat higher Fe concentrations than the composition of the starting mix. This is because of the unavoidable sputtering from the iron source holder as well as because there is a higher sputtering yield for Fe than for B. The films on glass were used for X-ray and SIMS analysis, while those on beryllium were generally used as Mössbauer absorbers. Low angle X-ray diffraction failed to show any structure in the films.

Secondary-ion mass spectrometry (SIMS) using a sputter ion source was used to analyze and determine the composition of the films. The instrument employed was a GCA IMS 101B (6). A defocused primary beam of 10keV Ar^+ was used to sputter the samples. Both polyatomic and atomic spectra were taken as sputter continued. From these spectra and those of bulk FeB compounds of known composition, information on film composition, homogeneity, and bonding state was obtained. It was found that the relative ion yield of boron and iron depends on the oxygen content of the films. When sputtering was done in a partial pressure of oxygen (10^{-5} Torr), these differences were found to be removed; accordingly, compositions were determined in oxygen. The results of SIMS analyses were used to point the way to refinements in film preparation which resulted in suitable films for Mössbauer studies. The films were found to be compositionally homogeneous to within 1 to 2% and total impurity levels (except for oxygen) were below 0.5%. Analysis of some of the Be substrate samples which were used for the Mössbauer studies indicates that there is a small variation in composition (± 1 to 2%) between various samples sputtered at the same time. Neither of the common iron oxides (Fe_2O_3 or Fe_3O_4) was observed in any of the Mössbauer spectra.

The ^{57}Fe Mössbauer spectra were obtained using a ^{57}Co in Rh source at the same temperature as the absorber, except in the 10K experiments where the source was at room temperature. In most experiments 2 or 3 beryllium disc absorbers were stacked to give a total film thickness of 5 to 10 μm. The slight differences in composition between the discs contributed a negligible amount of line broadening. The velocity spectrometer consists of a constant acceleration electromechanical transducer of conventional design together with a multichannel analyzer operated in the normalized mode for collecting and storing the data. Where the spectra are well resolved, they were analyzed by a least-squares fitting program to a sum of Lorentzian shaped lines - generally for absorbers above T_c, or where only non-magnetic spectra were observed.

 0021-8979/81/031808-03$1.10

The broadened magnetic spectra were analyzed using a version of Window's procedure for fitting a continuous distribution of magnetic hyperfine fields to a truncated cosine series expansion of P(H) (7). The instrumental (observed) line width (for the inner lines of a thin iron foil absorber) was less than 0.3 mm/sec.

RESULTS AND DISCUSSION

Mössbauer spectra of samples A, B, and C at 300K, 77K, and 10K are shown in Figure 1 (also C at 200K is shown). A qualitative evaluation of the spectra shows that atroom temperature the low Fe content samples (A and B) have a negligibly small (or zero) magnetic hyperfine structure. The asymmetrical, broadened, quadrupole split doublet is typical of disordered non-magnetic systems in which the asymmetry is generally thought to be due to a correlation between the isomer shift and the quadrupole splitting (8). The line widths (FWHM) of the quadrupole doublet components in Fig.1(a) and (d) are 0.503 $\pm$ .002 mm/sec; this is nearly double the line width that would be expected from a single site absorption line and indicates a distribution of quadrupole interactions and isomer shifts which is nevertheless narrow in comparison with the average quadrupole splitting. Some of the quadrupole splitting may be caused by strain in the films due to differences in expansion between the film and substrate. The room temperature values of isomer shift δ and quadrupole splitting ΔEq along with those for crystalline FeB are shown in Table I. For sample C, the value of ΔEq is derived from the splitting of the inner pair of lines without regard for the underlying magnetic hyperfine structure (hfs).

Relative to the room temperature isomer shift for α-Fe, the values for quenched alloys ($.72 \leq x \leq .86$) are positive and increase almost linearly with increasing boron content (1). This implies an increasing transfer of electrons from boron to the d-band of the alloy with increasing boron content (11). Though the values of δ for our samples ($0.40 \leq x \leq 0.50$) are experimentally indistinguishable from one another, the average value, $\delta = 0.22$ mm/sec, for the three alloys follows the above trend and thus indicates that the charge transfer per boron atom in the sputtered alloys occurs at about the same rate as in the quenched alloys.

Figure 1 shows that at77K the sample A ($x = .40$) spectrum is unchanged from that at 300K, except for a small increase in ΔEq; the line widths are the same at both temperatures, and there is no evidence of magnetic ordering. At 10K there is some broadening of the quadrupole components, but there is no indication of a hyperfine field greater than 40 kOe. The area under the split pair of quadrupole absorption lines, however, is less at 10K than at 77K; this could be due to a weak, very broad magnetic absorption spectrum which is buried in the counting statistics, or it may be an artifact of the low temperature experimental arrangement. The spectra of samples B ($x = .45$) and C ($x = .50$) show that an increasingly large fraction of the Fe sites becomes magnetically ordered as the temperature is lowered. At a fixed temperature below T_c, the fraction of magnetically ordered atoms increases as the Fe content is increased.

All the spectra have a distinct doublet near zero velocity, similar to the well resolved quadrupole doublet in Figure 1(a) where there is no evidence of a magnetic hfs. Curiously, the asymmetry of the doublet, in which the higher energy component (positive velocity) is more intense for the spectra without magnetic hfs, reverses in the presence of a large magnetic hfs. The presence of a large magnetic hfs, in which the quadrupole interaction can be treated as a perturbation, has the effect of averaging the angle θ between the EFG principal axis and the internal magnetic field direction, since the former direction is random in a disordered alloy, while the latter is correlated among atoms in a ferromagnetic domain (9). Below T_c, therefore, the magnetic hyperfine lines are broadened, but not shifted or made assymetric by the quadrupole interaction. It appears that the correlation between δ and ΔEq which exists above T_c is different below T_c. This is readily understandable in principle, since ΔEq and δ for a given Fe atom are both functions of the near-neighbor configuration surrounding that atom, and the near-neighbor configuration is also responsible for its magnetic state.

All the spectra were analyzed in terms of an effective distribution of hyperfine fields P(H), as described earlier (7). The important features for the present discussion are that the quadrupole doublet is always fitted by an equivalent P(H) distribution sharply peaked around 40 kOe with a FWHM of about 40 kOe. At higher hyperfine fields a P(H) representing magnetic atoms is observed which is peaked at values that are concentration and temperature dependent. There are a number of different ways of generating P(H) distributions from Mössbauer spectra, and the distributions described above are not meant to indicate more than the coarse features listed in Table II (10). The ratio of non-magnetic ($H \leq 40$ kOe) to magnetic ($H > 40$ kOe) atoms is given by the area under the first peak (low H) in the P(H) distribution divided by the total positive area under P(H).

The Fe atoms in crystalline FeB have a unique environment with a saturation magnetic hyperfine field of 131 kOe; it is difficult to explain the observed distribution of magnetic hyperfine fields in the amorphous $Fe_{.50}B_{.50}$ alloy without assuming that a large number of Fe atom environments are very different from the ones in crystalline FeB. The large difference in the values of electric quadrupole splitting (Table I) also points to the same conclusion, which is in contrast to the interpretation of results on liquid-quenched amorphous $Fe_{.75}B_{.25}$, where the local chemical order is believed to be the same as that in crystalline Fe_3B (5). These results suggest a structural model for the amorphous $Fe_{0.5}B_{0.5}$ alloy in which about 70% of the Fe atoms reside in regions having a local chemical order similar to crystalline FeB, with deviations around the crystalline bond lengths and angles. The remaining Fe sites may lie on the surfaces of these regions and thus, have local surroundings substantially different from crystalline. Such sites are either paramagnetic, non-magnetic,or possibly a combination of the two; their number increases as Fe content of the samples decreases (Table II).

ACKNOWLEDGMENT

The authors are pleased to acknowledge the capable assistance of J. W. Leight in preparing the sputtered films.

Table I. Isomer shifts (δ) and quadrupole splitting (ΔE_q) for samples A, B, C and crystalline FeB at room temperature (except FeB ΔE_q, see text). Isomer shifts are relative to α-Fe at 300K.

Sample	δ ($\frac{mm}{sec}$)	ΔE_q (mm/sec)
A - $Fe_{.40}B_{.60}$	+ 0.222 $\pm$ .01	0.600 $\pm$ .01
B - $Fe_{.45}B_{.55}$	+ 0.207 $\pm$ .01	0.575 $\pm$ .01
C - $Fe_{.50}B_{.50}$	+ 0.225 $\pm$ .01	0.639 $\pm$ .04
Crystalline FeB	+ .260	0.217 $\pm$ .008 (at 600K)

Table II. Fraction of Fe atoms having hyperfine fields $H \leq 40$ kOe, $f(0)$; and H_{peak} of the first prominent peak above the peak associated with the $H = 0$ quadrupole distribution. Values are obtained from the P(H) distributions for samples A, B and C at the indicated temperatures.

Sample	T(K)	f(0)	H (kOe) peak
A - $Fe_{.40}B_{.60}$	300	1.0	-
	77	0.9	-
	10	0.8	-
B - $Fe_{.45}B_{.55}$	300	1.0	-
	77	0.63	106.
	10	0.60	129.
C - $Fe_{.50}B_{.50}$	300	0.45	116.
	200	0.45	127.
	77	0.30	131.
	10	0.30	134.
Crystalline FeB	300	0.0	118.
	0	0.0	131.

REFERENCES

a) Work supported by the U.S. Army Research Office.
1. C. L. Chien et al., Phys. Rev. B 20, 293 (1979).
2. C. L. Chien, Phys. Rev. B. 18, 1003 (1978).
3. U. Gonser, M. Ghafari and H. G. Wagner, J. Magn. and Magn. Mater. 8, 175 (1978).
4. J. Balogh and I. Vincze, Solid State Commun. 25, 695 (1978).
5. I. Vincze, T. Kemény and S. Arajs, Phys. Rev. B. 21, 937 (1980).
6. R. F. K. Herzog, W. P. Poschrenrider and F. G. Satkiewicz, "Mass Spectrometer Analysis of Solid Materials with the Ion-Microprobe Sputter Source," NASA Report CR-683 (Jan., 1967).
7. B. Window, J. Phys. E. 4, 401 (1971).
8. C. L. Chien, J. Hyperfine Int. 4, 869 (1978).
9. T. E. Sharon and C. C. Tsuei, Phys. Rev. B. 5, 1047 (1972).
10. G. Le Caer and J. M. Dubois, J. Phys. E. 12, 1083 (1979).
11. L. R. Walker, G. K. Wertheim and V. Jaccarino, Phys. Rev. Lett. 6, 98 (1961).

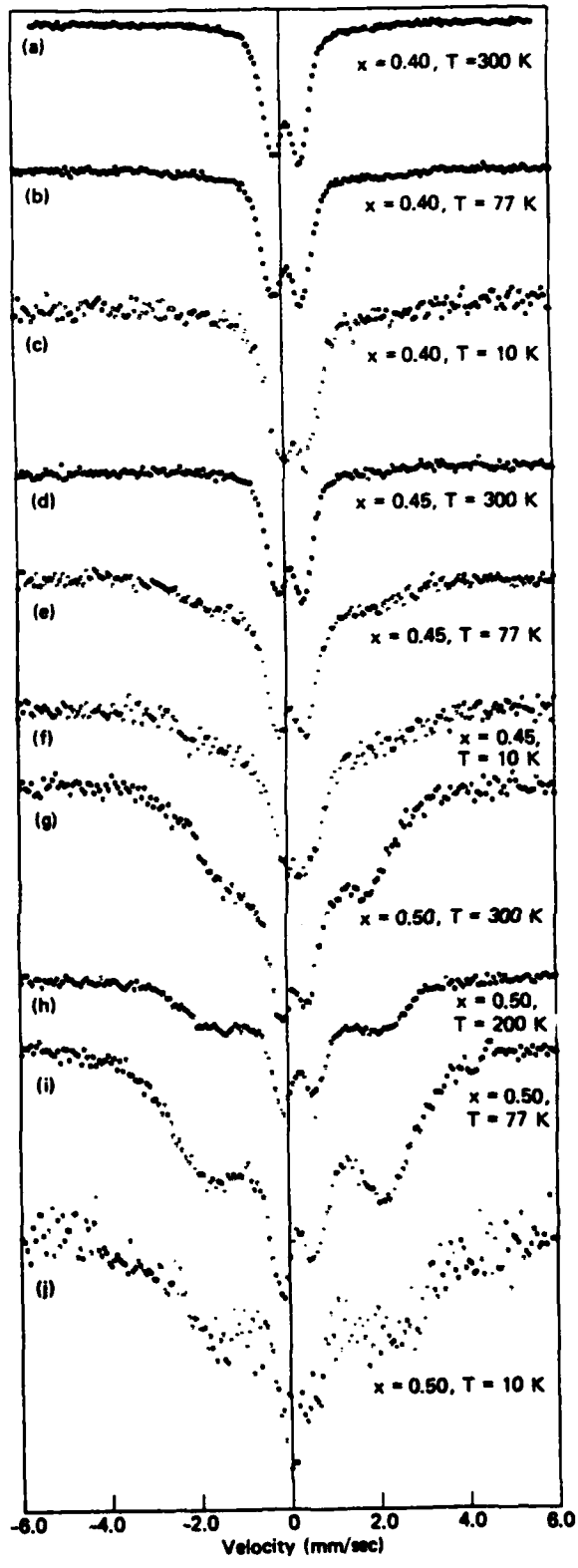

Fig. 1 Mossbauer spectra of $Fe_x B_{1-x}$ amorphous sputtered films for X = 0.40, 0.45, and 0.50 at various temperatures from 10 K to 300 K. Velocity scale is relative to ^{57}Co in Rh at the same temperature as the absorber, except at 10 K where the source is at room temperature.

APPENDIX 3

Mössbauer investigation of sputtered ferromagnetic amorphous Fe_xB_{100-x} films[a)]

N. A. Blum, K. Moorjani, T. O. Poehler, and F. G. Satkiewicz

The Johns Hopkins University, Applied Physics Laboratory, Laurel, Maryland 20707

Iron boride amorphous films were prepared by rf sputtering of polycrystalline FeB and Fe_2B powders. The films were analyzed for purity, uniformity, and composition by secondary ion mass spectrometry and were analyzed for lack of long range order by x-ray diffraction. As in the melt quenched alloys, Mössbauer spectra revealed a broad and nearly symmetric distribution of hyperfine fields in samples with a composition near a-Fe_2B. The hyperfine field distribution in samples with a composition near a-FeB, however, is asymmetric, and more significantly, reveals a large number of Fe sites with zero magnetic hyperfine field at temperatures down to 10 K. Analysis of the data throws light on the chemical short range order in the alloys.

PACS numbers: 75.50.Kj, 76.80. + y, 75.50.Bb

INTRODUCTION

Earlier findings that amorphous alloys may retain the chemical short range order of corresponding crystals (1), have been abundantly confirmed by a variety of techniques (2). In this paper we investigate chemical short range order in a-Fe_xB_{100-x} around concentration ranges of the stoichiometric compounds FeB, Fe_2B, and Fe_3B. Earlier studies (3,4) in the concentration range $72 \leq x \leq 86$ of the melt quenched alloys have shown that the chemical short range order for x = 75 is similar to that in crystalline Fe_3B (4), and that the ferromagnetic Curie temperature T_c of the alloys increases from approximately 550 K to 760 K as the iron concentration is decreased from 86 to 72 percent (3). Since the values of T_c for the compounds FeB and Fe_2B are approximately 600 K and 1000 K, respectively (5,6), it is expected that the above trend would be reversed for some concentration in the range $50 \leq x \leq 72$.

RESULTS

Thin film samples were prepared by rf sputtering of FeB and Fe_2B powders in an argon atmosphere onto thin (250 μm) beryllium foil discs. X ray diffraction was used to ascertain the amorphous nature of the samples, and secondary ion mass spectrometry (SIMS) was used to determine the composition and homogeneity of the films.

Mössbauer spectra were obtained using a ^{57}Co in Rh source at the same temperature as the absorber, except in the 10 K experiments where the source was at room temperature. Tabulated isomer shifts were calculated with respect to iron at 300 K. The broadened magnetic spectra were analyzed using a version of Window's procedure (7) for fitting a continuous distribution of magnetic hyperfine fields to a truncated cosine series expansion of P(H).

The room temperature spectrum of a-$Fe_{71}B_{29}$ is compared with the spectrum of Fe_2B powder in Fig. 1. The spectra are similar except for three prominent features which characterize nearly all the ferromagnetic amorphous film spectra: (a) the six spectral lines are greatly broadened in the amorphous alloy; (b) the $\Delta m = 0$ line intensities (lines 2 and 5) are quite different in the amorphous film compared with the crystalline powder; and (c) the amorphous film spectrum is noticeably asymmetric. The broadened lines reflect the distribution of hyperfine fields, and the line intensity ratios indicate that the iron magnetic moments in the amorphous alloy lie close to the plane of the substrate. In the randomly oriented powder the line intensities are close to the theoretical ratio, 3:2:1. In the amorphous alloy the intensity ratios are not immediately evident by inspection because of the distribution of hyperfine fields; however, analysis indicates that the ratio is close to 3:3.5:1; this places the average magnetization direction at room temperature about 15° out of the plane of the film. The asymmetry in the spectrum reflects the anisotropy of the hyperfine fields and perhaps a correlation between the isomer shift and/or the quadrupole splitting and the magnetic hyperfine field components.

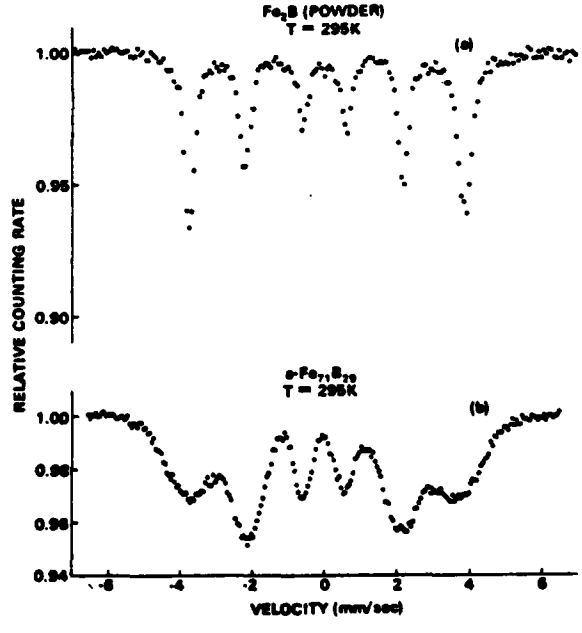

Fig. 1. (a) Spectrum of Fe_2B polycrystalline powder compared with (b) spectrum of a-$Fe_{71}B_{29}$ sputtered film, both at room temperature.

The spectra at 77 K and 10 K are similar to the room temperature spectrum, as are the P(H) distributions which are centered at a value near the Fe_2B hyperfine field, and are rather symmetrically distributed about that value. This differs from results on a-FeB, and points towards the existence of a similar chemical short range order in both the crystalline sample and in amorphous samples with a composition in the vicinity of Fe_2B.

 0021-8979/82/032074-03$02.40

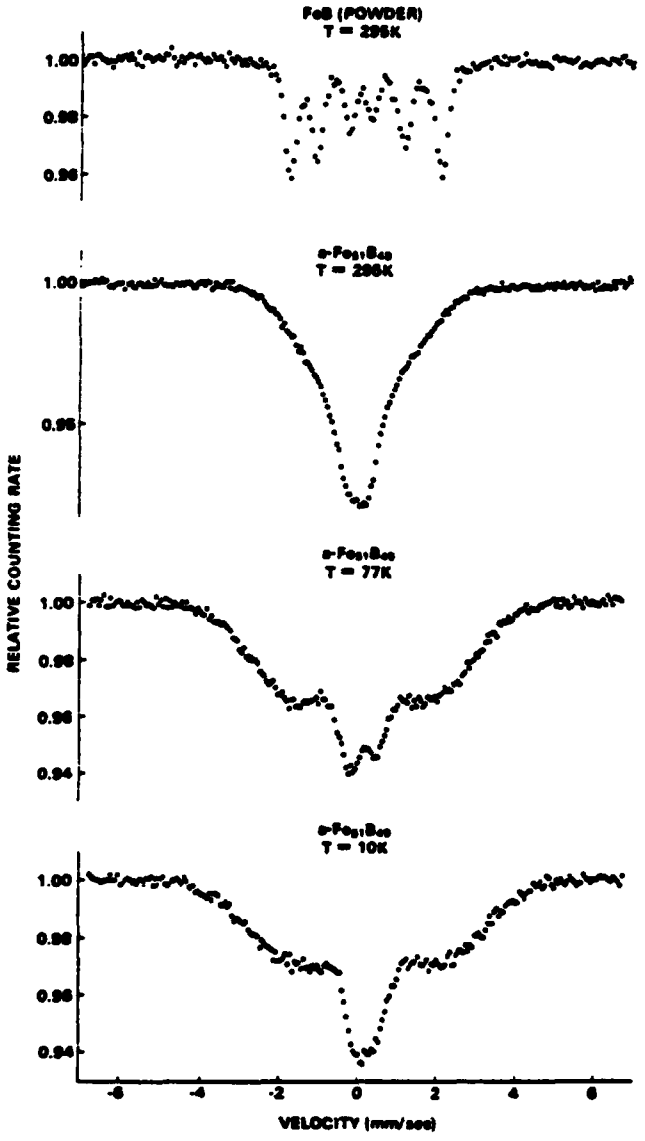

Fig. 2. Spectra of $a\text{-}Fe_{81}B_{19}$ sputtered film at various temperatures compared with FeB polycrystalline powder at room temperature.

Amorphous film samples in a range around x = 50 were prepared by sputtering FeB and mechanical mixtures of FeB plus B. Uniform films were produced with compositions between $Fe_{49}B_{51}$ and $Fe_{81}B_{19}$, as measured by SIMS. Figure 2 shows spectra of $Fe_{81}B_{19}$ at various temperatures compared with the spectrum of crystalline powder FeB at room temperature. Unlike Fe_2B, the amorphous sample spectrum is distinctly different from its crystalline counterpart. The P(H) fit shows a strong low field component plus a low amplitude distribution centered around 100 kOe. As the temperature is reduced (Fig. 2) the spectra show a broadly distributed magnetic field component (~ 100 kOe) increasing in both intensity and width. The lower peak in the spectrum, indicative of a low or zero field contribution, is present down to 10 K. The P(H) distributions show that the area under the higher field distribution becomes larger with decreasing temperature and that the peak of this distribution moves towards a higher magnetic field. At all temperatures there is a significant low field peak, encompassing the region approximately 0 to 60 kOe. All samples with less that about 50 percent iron have a distinct (partially resolved) quadrupole doublet near zero velocity (8). The quadrupole doublet persists below T_c in all samples, even down to 10 K. The quadrupole doublet (above T_c) can be fit by an equivalent P(H) distribution peaked about 40 kOe with a FWHM of about 40 kOe. This is an artifact of the fitting procedure in which the quadrupole doublet is interpreted as a distribution of six overlapping, magnetically split lines. The ratio of nonmagnetic (H < 60 kOe) to magnetic (H > 60 kOe) atoms may be obtained from the P(H) distributions. The fraction of nonmagnetic atoms at 10 K is approximately 30% and increases with temperature (8).

In Table I we list the isomer shifts, quadrupole splittings (measured above T_c), and the magnetic ordering temperatures (T_c) for the a-FeB series of samples, together with relevant parameter values of $a\text{-}Fe_2B$ samples and their crystalline counterparts. There is a significant isomer shift between a-FeB and $a\text{-}Fe_2B$ ($\Delta\delta$ = 0.10 mm/sec), showing that electrons are transferred to the d-band of the alloy with increasing boron concentration (9). The small differences in δ among the several a-FeB ($40 \leq x \leq 51$) and $a\text{-}Fe_2B$ ($71 \leq x \leq 80$) samples are within the experimental errors of the measurements (~ .02 mm/sec). One might expect some structural differences between melt-quenched and sputtered alloys; however, the accuracy of the present data is inadequate to support or reject this view.

Table I. Isomer shifts (δ) and quadrupole splittings (ΔE_Q) at room temperature (except as noted), and values of magnetic transition temperature (T_c) for several sputtered amorphous films, melt quenched (m.q.) ribbons and stoichiometric crystalline compounds. The sputtered amorphous film values are from this paper; the others are from the references.

Sample	δ (mm/sec)	ΔE_Q (mm/sec)	T_c (K)
$a\text{-}Fe_{49}B_{51}$ (sputtered)	+0.22	0.60	< 10
$a\text{-}Fe_{45}B_{55}$ (sputtered)	+0.21	0.58	~ 100
$a\text{-}Fe_{50}B_{50}$ (sputtered)	+0.23	0.64	≥ 350
$a\text{-}Fe_{81}B_{19}$ (sputtered)	+0.22	0.54 (at 150K)	375
cryst. FeB (Ref.5)	+0.26	0.22 (at 600K)	600
$a\text{-}Fe_{71}B_{29}$ (sputtered)	+0.12	-	≥ 750
$a\text{-}Fe_{80}B_{20}$ (m.q.,Ref.3)	+0.09	-	685
$a\text{-}Fe_{72}B_{28}$ (m.q.,Ref.3)	+0.07	-	760
cryst. Fe_2B (Ref.6)	+0.12	-	1015
cryst. Fe_3B (Ref.3)	+0.05 to +0.14	-	~ 820

At temperatures above room temperature the quadrupole doublet (unresolved in Fig. 2) becomes partially resolved. Assuming that the entire spectrum is composed of two lines (a quadrupole doublet), a plot of the average line width of the two lines as a function of temperature indicates the temperature at which the broadening due to the magnetic background disappears; this gives a value T_c = 375 K for $a\text{-}Fe_{81}B_{19}$. As expected, the trend towards higher T_c with decreasing Fe content (3) reverses somewhere between 51 and 71 percent Fe.

CONCLUSIONS

In order to explain the observed distribution of magnetic hyperfine fields in the amorphous FeB alloys, one must conclude that a large number of Fe atom environments are very different from the ones in crystalline FeB. Our results suggest a structural model for amorphous FeB alloys in which up to 70 percent of the Fe atoms reside on sites having local chemical order similar to the crystalline state, with deviations around the crystalline bond lengths and angles. The remaining 30 percent (nonmagnetic) Fe sites may lie in local surroundings substantially different from the crystalline ones. Such sites are either paramagnetic, nonmagnetic, or possibly a combination of the two; their number increases as the Fe content decreases. In contrast to the results for a-FeB, a-Fe_2B appears to have chemical ordering similar to the crystalline state.

ACKNOWLEDGMENT

The authors acknowledge the capable assistance of J. W. Leight in preparing the sputtered films.

REFERENCES

a) Work partially supported by the U. S. Army Research Office.
1) J. F. Sadoc and J. Dixmier, Mat. Sci. Eng. 23, 187, 1976.
2) J. Durand, Proc. 4th Int'l. Conf. Liquid and Amorphous Metals, J. Physique 41, 609, Colloque C8, 1980.
3) C. L. Chien, D. Musser, E. M. Gyorgy, R. C. Sherwood, H. S. Chen, F. E. Luborsky, and J. L. Walter, Phys. Rev. B 20, 283, 1979.
4) I. Vincze, T. Kemeny and S. Arajs, Phys. Rev. B 21, 937, 1980.
5) J. E. Jeffries and N. Hershkowitz, Phys. Lett. 30A, 187, 1969.
6) K. A. Murphy and N. Hershkowitz, Phys. Rev. B 7, 23, 1973.
7) B. Window, J. Phys. E 4, 401, 1971.
8) N. A. Blum, K. Moorjani, T. O. Poehler, and F. G. Satkiewicz, J. Appl. Phys. 52, 1808, 1981.
9) L. R. Walker, G. K. Wertheim and V. Jaccarino, Phys. Rev. Lett. 6, 98, 1961.

APPENDIX 4

Solid State Communications, Vol.43,No.4, pp.239-242, 1982.
Printed in Great Britain.

0038-1098/82/280239-04$03.00/0
Pergamon Press Ltd.

SPIN GLASS BEHAVIOR AND NON-ERGODICITY IN AMORPHOUS IRON-BORON ALLOYS*

D. J. Webb** and S. M. Bhagat

Dept. of Physics and Astronomy, Univ. of Maryland, College Park, MD 20742 U.S.A.

and

K. Moorjani, T.O. Poehler, and F. G. Satkiewicz
The Johns Hopkins University
Applied Physics Laboratory
John Hopkins Road
Laurel, Maryland 20707, U. S. A.

Received 20 March 1982 by E.F. BERTAUT

We report FMR measurements on amorphous Fe_xB_{1-x} thin films with x=0.47,0.49 and 0.53. At low T we observe anomalies characteristic of the FM-SG transition. In addition, in the 0.47 and 0.49 alloys the resonance field, below ~80K, depends upon the rate of cooling. We suggest that this behavior is symptomatic of non-ergodicity in the spin glass state.

Introduction

Crystalline and amorphous alloys of the type M_xG_{1-x}, where M denotes one or more magnetic moment carrying transition metal atoms, and G represents glass formers or noble metals, have been intensively investigated recently.[1] Several[2-6] independent studies have established the re-entrant magnetic behavior of these alloys at values of x slightly larger than that required for the onset of ferromagnetism. That is, when the temperature is lowered, the alloys first exhibit the usual paramagnetic-ferromagnetic transition at a Curie temperature T_c. However, on further lowering of the temperature a transition to the spin glass state, in which the spins freeze in random directions with no net long range magnetic order, is observed at a well defined temperature T_f.

Systematic ferromagnetic resonance (FMR) measurements on amorphous re-entrant alloys reveal several characteristic features:[7] a) At low temperatures the linewidths (Γ) increase rapidly with decreasing temperature and in some cases exhibit maxima. This is in contrast to ordinary ferromagnetic alloys where, at low temperatures, Γ is independent of temperature; b) The magnetization, M, derived from the resonance center, H_r, shows an anomalous behavior at low temperatures in that marked deviations from the usual $T^{3/2}$ behavior are observed for the re-entrant alloys. The same alloys in the ferromagnetic range (i.e., higher values of x) indeed show the $T^{3/2}$ behavior at low temperature; c) these anomalies arise at temperatures that are well above T_f and bear no simple relation to it.

In this paper, we report FMR measurements on amorphous binary alloys Fe_xB_{1-x} with x in the vicinity of 0.5, i.e., about 0.1 higher than that required for onset of ferromagnetism. In addition to exhibiting the aforementioned anomalies showing the persistence of the spin glass behavior in amorphous alloys with only one magnetic component, the existence of several metastable states due to the non-ergodic nature of spin glasses[8] is demonstrated. These metastable states are characterized by differing values of H_r which depend on the rate of cooling below 80 K.

Experimental

The samples were prepared by rf sputtering of FeB and mixtures of FeB and B onto quartz substrates. A special magnetic focussing ring was used to confine the sputtering ions so as to enhance the sputtering rates. That the films are indeed chemically homogeneous was confirmed by the sputter-ion mass spectrometer which also gave their chemical composition. The concentration range ($0.47 \lesssim x \lesssim 0.53$) studied in the present work is slightly above the critical concentration for the onset of ferromagnetism in these alloys[9] and brackets the concentration for which the crystalline alloy, FeB, is a strong

*Research at Johns Hopkins partially supported by the U. S. Army Research Office

**From a disertation to be submitted to the Graduate School, University of Maryland, by D.J.W. in partial fulfillment of the requirements of the Ph.D. degree in Physics.

ferromagnet[10] with T_c = 598 K. Similar amorphous alloys have been previously investigated by Mössbauer spectroscopy.[11]

Most of the present FMR measurements were conducted in the parallel geometry ($H_{d.c.} \parallel$ to sample plane) at approximately 11 GHz and 35 GHz in the temperature range 2-300 K. Using the equation, $(\omega/\gamma)^2 = H_r(H_r + 4\pi M)$, the H_r data were used to evaluate $4\pi M$ as well as the g-value which, along with other parameters of the alloys, are listed in Table I. At a few temperatures H_r was measured as a function of the angle between the sample plane and the applied field. This provided further checks on the values of g and M.

The present results follow the trend reported in Ref. 12, i.e., Fe moment reduces monotonically with reducing x.

The temperature dependence of the observed linewidths at 11 GHz, presented in Fig. 2, clearly shows the anomalous behavior at low temperatures and in particular the linewidth for the Fe_{47} alloy exhibits a maximum such as previously reported for low x alloys in other reentrant systems.[7,14]

For the present discussion, the results of greatest interest come from noting the peculiar low temperature dependence of H_r in the Fe_{49} and Fe_{47} alloys at 11 GHz. For instance, the tem-

Table I Magnetic Parameters of Fe_xB_{1-x} Alloys

Sample	Conc.	T_c[a] (K)	$4\pi M_o$ (kOe)	g	B × 10^{-5} $(K)^{-3/2}$	μ_B/F
Fe_{53}	$Fe_{0.53}B_{0.47}$	560	6.5	2.07	7.4	0.87
Fe_{49}	$Fe_{0.49}B_{0.51}$	452	5.5†	2.05*	6.8	0.78
Fe_{47}	$Fe_{0.47}B_{0.53}$	384	4.95†	2.09*	7.6	0.71
xtal FeB		598[b]	-	-	-	1.1[c]

a. deduced from empirical relation $T_c = 4 \times 10^3(x - 0.38)$ following Ref. 9

* for 80 < T < ..0 K (Fig. 1)

† extrapolated (see Fig. 1)

b. Ref. 10

c. Ref. 13

d. assumed density $\delta = 7$ gm-cm^{-3}

Results and Discussion

The temperature dependence of the magnetization, derived from the H_r data, is presented in Fig. 1. Apart from slight deviations below ~20 K, the conventional behavior, $M = M_o(1 - BT^{3/2})$, due to the excitation of spin waves, is a good representation of the data for Fe_{53} over the entire temperature range, that is, up to $T/T_c \approx 0.54$. For the other two alloys, the $T^{3/2}$ dependence is observed only for T ≥ 80 K. Over these temperature ranges the g values, given in Table I, are independent of T. At lower T (see below) the variation in H_r becomes more complex and one cannot assign meaningful values to g and M without introducing additional parameters.

The observed values of B, also listed in Table I, are somewhat larger than those reported for other amorphous alloys of comparable Fe content[7,13] which indicates somewhat weaker exchange interaction in the present alloys. It should also be noted that for the Fe_{53} alloy, where $4\pi M_o$ has a straightforward meaning, the Fe moment is 0.87 μB/atom which is to be compared with the value[13] 1.1 μB/atom for crystalline FeB. For the other two alloys, the zero Kelvin intercept is harder to interpret but if we treat the M_o values as above, the values 0.78 μB/atom and 0.71 μB/atom are obtained for Fe_{49} and Fe_{47} alloys, respectively.

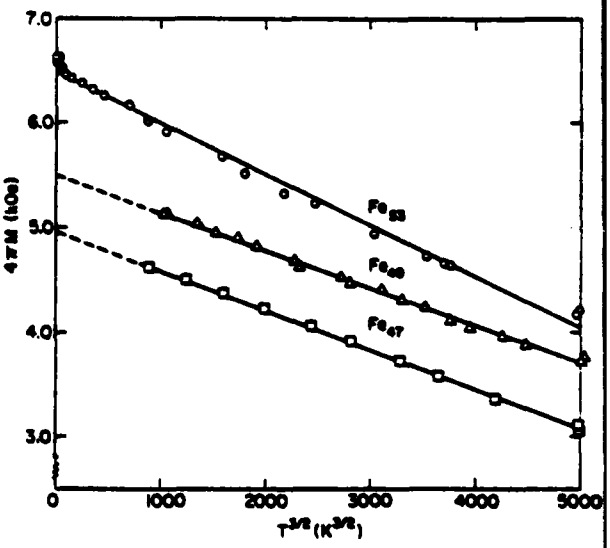

Fig. 1. Temperature dependence of the magnetization deduced from FMR data on amorphous Fe_xB_{1-x} alloys. As descr... in the text, below 80 K, Fe_{47} and Fe_{49} do not show simple behavior. Hence, the dashed lines.

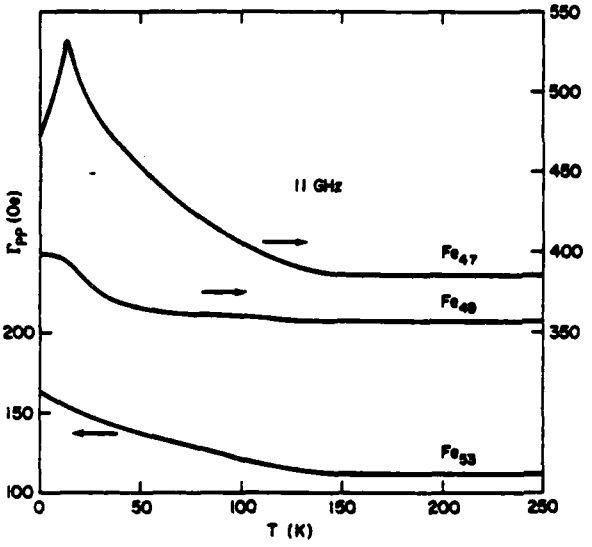

Fig. 2. Temperature dependence of the FMR linewidths at 11 GHz for amorphous Fe_xB_{1-x} alloys.

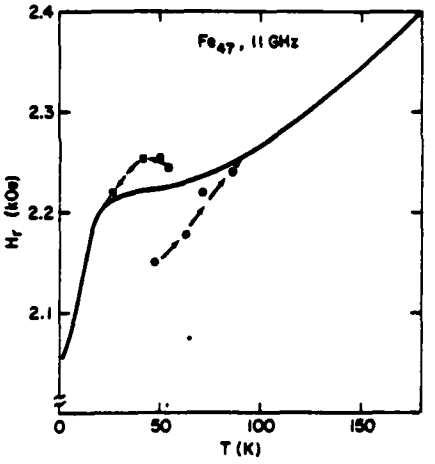

Fig. 3. Temperature dependence of the resonance field for FMR in amorphous Fe_{47}. As described in the text, below 80 K, the data are dependent upon the thermal history: the solid line is obtained on slow (~0.25 K/min) cooling while the other data represent other thermal cycles (see text).

perature dependence of H_r at 11 GHz for Fe_{47} at three different cooling rates below ~80 K is shown in Fig. 3 and can be described as follows: a) The solid line represents what we choose to designate the equilibrium state obtained either by cooling slowly (~0.25 K/min) or by cooling in zero field directly to 4 K and observing H_r during a subsequent warming. From several such runs we deduce that the H_r values are good to about 10 Oe. b) When the sample was first cooled rapidly (~2 K/min) from 80 K to 50 K, the H_r values represented by the solid circles were observed during a subsequent warm-up. The warming could be carried out quite slowly without affecting the H_r data. c) In another run, the cooling between 80 K and 50 K was carried out in ten minutes, followed by a slow cool to lower temperatures. The H_r values shown as full squares were observed.

For other cooling cycles H_r values between these extremes have been seen. In these intermediate states, however, slight changes in temperature cause the system to return to the equilibrium curve. It should be noted that the linewidths are roughly the same for all cooling cycles. Although we are implying that the particular values of H_r, other than the equilibrium values, are symptomatic of metastable states in the spin freezing process, at this time we do not know precisely how the cooling rate controls the specific state in which the system finds itself.

It has been known for some time that anisotropy fields develop when there is a transition from the paramagnetic to the spin glass phase[15,16], and recently similar anisotropy fields have been shown to accompany the ferromagnet-spin glass transition.[17] For the equilibrium curve, the sharp decrease in H_r around 20 K is ascribed to this effect. If in the freezing process the spin system has access to other states of metastable equilibrium (i.e., local free energy minima) it is not surprising that, on occasion, it finds itself trapped in one of these configurations and consequently the anisotropy fields, or H_r, differ from the equilibrium value. The results clearly lend support to the recent suggestion[8] that the spin glass state is inherently non-ergodic in character. That is, there exist many equivalent free energy minima with significant barriers between them so that some of the minima are inaccessible during the approach to equilibrium. Thus it may happen that the system gets metastably locked into a state of "local" equilibrium in which the spin configurations and the consequent internal fields are significantly different from those in the "true" equilibrium state. Further work is being done to study the type of thermal effects shown in Fig. 3 at other microwave frequencies and different x values.

Acknolwedgments -- The capable assistance of J. W. Leight in preparing the samples is thankfully acknowledged. We are also thankful to M. Manheimer for several fruitful comments.

References

1. Recent reviews include J. A. Mydosh and G. J. Nieuwenhuys, in "Ferromagnetic Materials," Ed. E. P. Wohlfarth, North Holland Publishing Co., Amsterdam (1980), Vol. 1, p. 71.
2. B. H. Verbeek, G. J. Nieuwenhuys, H. Stocker, and J. A. Mydosh, Physical Review Letters 40, 586 (1978).
3. J. A. Geohegan and S. M. Bhagat, Journal of Magnetism and Magnetic Materials 25, 17 (1981).
4. Y. Yeshurun, M. B. Salamon, K. V. Rao, and H. S. Chen, Physical Review B24 1536 (1981)
5. S. Crane and H. Claus, Physical Review Letters 46, 1693 (1981).
6. J. W. Lynn, R. Erwin, J. J. Rhyne and H. S. Chen, Journal of Applied Physics 52, 1738 (1981).
7. M. L. Spano and S. M. Bhagat, Journal of Magnetism and Magnetic Materials 24, 143 (1981).
8. P. W. Anderson, "Ill-Condensed Matter," ed. R. Babian, R. Maynard, and G. Toulouse, North Holland (1978), p.159; A. Blandin, Journal of Physics (Paris), Colloquia 39, C6-1499 (1978).
9. C. L. Chien and K. M. Unruh, Physical Review B24, 1556 (1981).
10. N. Lundquist, H. P. Myers and R. Weshu, Philosophical Magazine 7, 1197 (1962).
11. V. Blum, K. Moorjani, F. G. Stakiewicz, and T. O. Poehler, Journal of Applied Physics 52, 1808 (1981). Ibid (1982), to be published.
12. R. Hasegawa and R. Ray, Physical Review B20, 211 (1979).
13. T. Shinjo, F. Itoh, H. Takahi, Y. Nakamura and Y. Shikazono, Journal of Physical Society (Japan) 19, 1252 (1964).
14. B. R. Coles, B. V. B. Sarkissian, and R. H. Taylor, Philosophical Magazine B37, 489 (1978).
15. S. Schultz, E. M. Gullikson, D. R. Fredkin and M. Tovar, Physical Review Letters 45, 1508 (1980).
16. P. Monod and Y. Berthier, Journal of Magnetism and Magnetic Materials 15-18, 149 (1980).
17. M. Manheimer, S. M. Bhagat, L. M. Kistler, and K. V. Rao, paper No. GE-8, 27th Annual Conference on Magnetism and Magnetic Materials, Atlanta, November 1981. Journal of Applied Physics (in press).

APPENDIX 5

J. Appl. Phys. (to be publishe

Mössbauer study of magnetism in an amorphous $Fe_{40}B_{60}$ sputtered film[a)]

W. A. Blum

The Johns Hopkins University, Applied Physics Laboratory,

Laurel, Maryland 20707

ABSTRACT

Mössbauer studies of amorphous iron/boron alloys have proved useful for understanding magnetic phenomena in structurally disordered systems. In iron-rich alloys the ^{57}Fe Mössbauer spectra at $T \ll T_c$ of both melt-quenched and sputtered materials consist of broadened magnetic hyperfine lines, indicative of structural distortions in the compounds Fe_2B and Fe_3B. The spectra of sputtered films with approximately 50% Fe may be characterized by two qualitatively distinct Fe sites: (1) sites yielding a broadened magnetic hyperfine spectrum similar to the sharp spectrum of the compound FeB, and (2) sites having a zero (or very small) magnetic hyperfine field, evidenced by a slightly asymmetric, partially resolved, quadruple doublet. In order to further examine the nature of these low field sites, a 40% Fe sputtered amorphous film was examined at 4.2 K in external magnetic fields up to 8.0 T. Interpretation is difficult, partly because the magnetic and quadrupole interactions are of comparable magnitude and partly because of the distributed nature of the hyperfine parameters. A pure spin-glass phase was ruled out by a narrowing of the spectrum in a 2.0 T external magnetic field. Two components were identified in the external magnetic field spectra: (1) non-magnetic (~ 50%), and (2) magnetic, with unusual behavior that may be due to a low-moment, mixed ferromagnetic/spin-glass phase.

PACS numbers: 75.50.Kj, 76.80.+y, 75.25+z

INTRODUCTION

Previous Mössbauer studies of sputtered, amorphous, Fe_xB_{100-x} films with approximately 40 to 50 at.% Fe indicate that at temperatures well below the magnetic ordering temperature T_c the spectra may be fit by a magnetic hyperfine field distribution P(H). This distribution is qualitatively characterized by a broad, structureless peak with a maximum near 120 kOe at x = 50, shifting towards lower H values with decreasing Fe concentration [1]. Another peak has been observed in the P(H) distribution that has a maximum near 30 kOe; this peak increases in intensity with decreasing Fe concentration, but the maximum of the peak remains near 30 kOe [2,3]. This low field peak is not observed in sputtered films with $x \gtrsim 60$, nor in any of the melt-quenched, iron/boron, amorphous alloys. It appears to be essentially the same as the peak seen in the P(H) derived from spectra obtained above T_c, where it is clearly just an artifact of the computational procedure [4,5] in which the broadened quadrupole doublet is fit by an equivalent magnetic field distribution. A representative example is shown in Fig. 1, for $Fe_{53}B_{47}$, where the optimized P(H) distribution shows two clearly defined maxima at about 30 and 120 kOe. The implication, as pointed out elsewhere [2], is that there are two types of Fe sites in these samples: (a) sites with a mean magnetic hyperfine field close to the value in crystalline FeB, and (b) low, or zero field sites substantially different from the crystalline ones. This paper reports on the nature of these low field sites by examining the interaction with an external magnetic field. For this purpose, a sample with a composition close to the threshold for magnetic ordering (~ 40% Fe) [1] was used in order to minimize interference in the Mössbauer spectra from the inner lines of the strongly magnetic components.

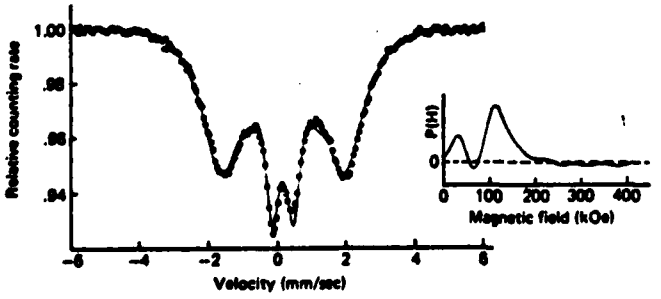

Fig. 1. Mössbauer spectrum and least squares optimized magnetic hyperfine field distribution P(H) for sputtered amorphous $Fe_{53}B_{47}$ film at T = 295 K.

EXPERIMENTAL

Amorphous iron/boron thin films were deposited in an rf diode sputtering system having a base pressure in the mid - 10^{-7} Torr range. Argon was used as the sputtering gas, throttled during deposition to a pressure of about 5 μm. The sputtering target was a mechanical mixture of commercially obtained 99% pure FeB and 99.7% pure boron powders packed into an iron target holder dish. The atomic composition of the target powder mix was nominally $Fe_{38}B_{62}$; secondary ion mass spectrometry (SIMS) analysis of the sputtered films gave a composition of $Fe_{40}B_{60}$ with good homogeneity. Three samples prepared at the same time, each alloy layer 3 to 5 μm thick on a Kapton polyimide film substrate, were mounted together to form the Mössbauer absorber used in the experiments reported here. Lack of long range order was ascertained by x-ray diffraction on similarly prepared samples deposited on glass.

The Mössbauer spectra were obtained with both the ^{57}Co in Rh source and the amorphous $Fe_{40}B_{60}$ absorber at the same temperature (4.2 K in the magnetic field experiments). The spectrometer is a conventional constant acceleration electromechanical velocity modulator used in conjunction with a multichannel analyzer/computer for collecting and analyzing the data. The magnetic field experiments were performed at the MIT Francis Bitter National Magnet Laboratory using a superconducting solenoid. A reverse winding on the solenoid kept the magnetic field at the source near zero.

The magnetic hyperfine field distributions P(H) were obtained using a version of Window's procedure for fitting a continuous distribution of magnetic fields to

a truncated cosine series expansion in H [4,5]. Asymmetries in the spectra are due to correlations between isomer shift, quadrupole interaction, and magnetic interaction. The P(H) program symmetrizes the spectra and does not explicitly consider isomer shift and quadrupole splitting distributions. In the present implementation of this procedure the relative intensities of the $\Delta m = 0$ lines were allowed to vary between 0 and 3.5 to obtain the best least squares fit. The intensity ratios of the outer to inner lines were fixed at 2.6 because thin (2-5 μm), sputtered, pure iron foils least squares fit with Lorentzian lines of width 0.28 to 0.30 mm/sec showed outer-to-inner intensity ratios (also area ratios) of 2.6:1. For well defined spectra (higher Fe concentration), using an outer/inner ratio of 2.6 gave better fits than using the theoretical ratio of 3.0.

RESULTS

The spectra of $Fe_{\sim 80}B_{\sim 20}$ in zero external magnetic field together with plots of the derived internal magnetic field distributions at 77 K and 4.2 K are shown in Fig. 2. The quadrupole splitting at 77 K is ΔQ = 0.62 mm/sec. At 295 K and 10 K (not shown) the spectra are nearly identical to those at 77 K and 4.2 K, respectively, indicating that the magnetic ordering temperature T_c is between 10 K and 77 K. The peak at 24 kOe in the 77 K P(H) distribution is a computational artifact in which the quadrupole doublet is interpreted as an equivalent magnetically split spectrum. At 4.2 K the P(H) peak broadens and moves to higher field. This is a manifestation of the appearance of an internal magnetic hyperfine field H_{int} below T_c. Since the magnetic P(H) and the component due to the quadrupole splitting overlap, it is not possible to extract simply the magnetic P(H) from the mixed electric quadrupole/magnetic dipole interactions. Indication of a significant distribution of quadrupole splitting is evident from the line widths in Fig. 2a (0.50 mm/sec), and also from an inability to fit the spectrum with Lorentzian shaped lines. The spectrum asymmetry further indicates that the quadrupole splitting is correlated with isomer shift. The average isomer shift at 4.2 K is δ = +0.11 mm/sec, and is independent of external magnetic field.

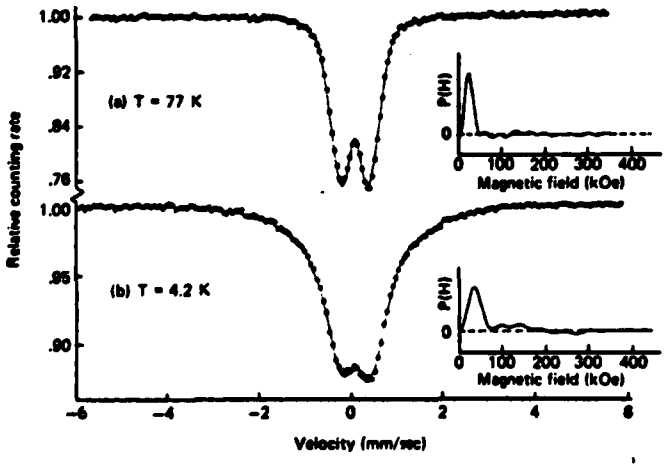

Fig. 2. Mössbauer spectra and P(H) distributions for sputtered amorphous $Fe_{\sim 80}B_{\sim 20}$ film at (a) 77 K and (b) 4.2 K; H_{app} = 0.

The spectra in external magnetic fields H_{app}, colinear with the γ-ray direction, and plots of derived least squares P(H)'s are shown in Fig. 3. The solid lines in the spectra correspond to the least-squares fit. The arrows beneath the spectra indicate the positions of the centers of the outer spectral lines corresponding to H_{app}. In an external field, P($\vec{H}$) is understood to be P($|\vec{H}_n|$), where the vector sum $\vec{H} = \vec{H}_{int} + \vec{H}_{app}$ is the net (observed) magnetic field.

The appearance of the spectra at all external fields indicates the presence of a net magnetic field component close in magnitude to the applied field. At the same time, the region of the spectrum corresponding to zero (or small) net magnetic field remains intensified beyond what it would be if the applied field (broadened by the internal field distribution and quadrupole distribution) were the only net field. Table I gives the peak positions and widths for all of the P(H) distributions shown in Fig. 2 and 3. The fourth column of the Table will be explained later.

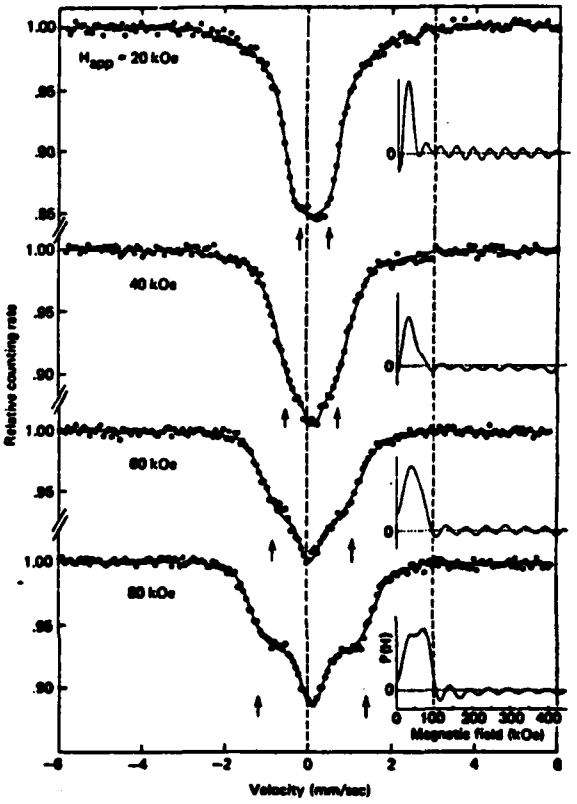

Fig. 3. Mössbauer spectra and P(H) distributions for sputtered amorphous $Fe_{\sim 80}B_{\sim 20}$ film at 4.2 K and several values of H_{app}. The arrows indicate the outer line positions corresponding to the applied magnetic field.

A qualitative description of the effects on the spectra of the external magnetic field follows (refer to Fig.3): The spectrum narrows upon the application of 20 kOe, and is characterized by a P(H) at 40 kOe similar to the P(H) at 0 kOe. At 60 kOe the peak shifts upwards and broadens. At H_{app} = 80 kOe two peaks can be resolved in the P(H): one at 35 kOe and the other at 72 kOe, both of about the same width. If one assumes two equal width, gaussian shaped peaks, the peak positions (unfolded) lie near 34 and 74 kOe. The lower applied field P(H) distributions could similarly be split, less convincingly to be sure, into overlapping distributions corresponding to H = 0 (appears to be a peak at 32 kOe due to the quadrupole doublet) and a peak near $H = H_{app}$. In the H_{app} = 80 kOe spectrum, the partially resolved peaks lend a degree of credibility to the interpretation that there are basically two components observed in the spectra: one characterized by the magnitude of the applied field and the other by a lower field distribution that crosses through H_n = 0 kOe near H_{app} = 20 kOe, and increases to about H_n = 34 kOe at H_{app} = 80 kOe.

DISCUSSION

The P(H) distributions, especially the one at H_{app} = 80 kOe showing resolved peaks at H_n = 34 and 74 kOe,

imply that there are at least two magnetic sites: one essentially non-magnetic, giving $H_n = H_{app}$; and the other magnetic in the sense that there is an internal contribution to the hyperfine field. The considerable width of the 74 kOe peak may be due to two causes: (1) the combined quadrupole/magnetic interaction, and (2) the finite resolution of the computational method. That the peak at H_n = 74 kOe occurs at a value less than the applied field is attributed to a small demagnetizing field and to lack of knowledge concerning the separate shapes of the two distributions: the low field distribution may have a tail, shifting lower the apparent position of the higher peak.

Table I. Position of peaks and widths of P(H) distributions for $Fe_{40}B_{60}$ at various external magnetic fields. T = 4.2 K, except for the first entry. The fourth column lists the peaks of the P(H) distributions for the stripped spectra (see text).

	Experimental		Stripped
H_{app} (kOe)	H_{peak} (kOe)	Width (kOe)	H_{peak} (kOe)
0 (77 K)	24	21	-
0	33	35	(33)
20	25	22	31
40	32	35	31
60	40	60	31
80	34/74	40/40	38

Analysis is exacerbated by the distributed nature of all the fundamental interactions: isomer shift, quadrupole splitting, and magnetic splitting. Not only are these interactions distributed, but the shapes of the distributions are *a priori* unknown. Since the spectrum initially narrows on application of an external magnetic field (20 kOe), it is clear that there are iron moments aligned with the external field (the internal field direction is opposite to the magnetic moment direction), i.e. there is a magnetic component. The average quadrupole splitting (~ 0.6 mm/sec) is equal to the ^{57}Fe, I = 3/2, excited state magnetic splitting at 90 kOe. The spectra thus are in the regime of mixed electric quadrupole/magnetic dipole interactions of comparable magnitude, precluding the usual perturbation approach.

An alternative to analyzing the spectra by studying the P(H)'s is to generate a theoretical spectrum, using the exact Hamiltonian for the mixed interaction [6,7], and averaging over all angles between the fixed external magnetic field direction (colinear with the γ-ray direction) and the direction of the EFG principal axis. In doing this, it is appropriate to use as generating parameters the experimental quadrupole doublet line width (above T_c) to account for the distribution of quadrupole interactions and isomer shifts, the observed quadrupole splitting, and the applied magnetic field. The computer generated spectrum is then normalized and subtracted from the observed spectrum by matching the theoretical and experimental spectra in the outermost extremities (wings). As in the P(H) analysis, the method is much more convincing in the H_{app} = 80 kOe case than in the lower field experiments. The result (for the 80 kOe case) is that somewhat more than half the area under the spectrum corresponds to just the applied magnetic field, broadened and distorted by the quadrupole distribution. The remainder of the spectrum contains no structure (like the H_{app} = 40 kOe spectrum) and gives a P(H) with an observed peak at H_n = 38 kOe.

Similarly, theoretical spectra for the other applied fields were generated and subtracted from the experimental data. The resulting "stripped" spectra were fit by P(H) distributions, the peak values of which are listed in the last column of Table I. The stripped spectra appear to be nearly shielded from the external field; this behavior is inconsistent with simple ferromagnetism. The distribution peaks near 30 kOe are not readily interpreted in detail because of the unknown contributions of the quadrupole and isomer shift distributions. About the only conclusion that may be drawn in each case is that the internal magnetic field (for this component of the spectrum) is less than 30 kOe, and may be close to zero.

One might anticipate the possibility that at 4.2 K the iron moments are in a spin-glass phase. There is evidence of this in the recent FMR experiments of Webb et al., where sputtered, ~50% Fe samples show line width anomalies at low temperature that are characteristic of spin-glass behavior [8]. In an external magnetic field the position of the peak of the P(H) of a spin-glass would increase, and the width would also increase. Quite the opposite is observed when H_{app} = 20 kOe (Fig.3). Unless the spin-glass state is destroyed by the 20 kOe applied field, amorphous $Fe_{40}B_{60}$ at 4.2 K is not simply a spin-glass. The observed behavior of the low field components may be due to the coexistence of low-moment ferromagnetic and spin-glass phases [9]. The (small) internal field associated with the ferromagnetic phase subtracts from the applied field, while the spin-glass phase contributes a slow broadening and increase in the peak position of P(H).

In summary, external magnetic field experiments on amorphous, sputtered $Fe_{40}B_{60}$ identify two types of iron sites: (1) non-magnetic (magnetic moment close to zero), and (2) magnetic (having a distribution of magnetic moments) - possibly a low-moment, mixed ferromagnetic/spin-glass phase.

ACKNOWLEDGMENTS

The magnetic field experiments were performed at the MIT Francis Bitter National Magnat Laboratory with the collaboration of R. B. Frankel and G. C. Papaefthymiou, to whom the author is especially grateful. The author also thanks C. L. Chien, C. Feldman, A. N. Jette, J. W. Leight, K. Moorjani and F. G. Satkiewicz for helpful advice, discussion and assistance.

REFERENCES

a) Work supported by the U. S. Army Research Office and the U. S. Naval Sea Systems Command under Contract No. N00024-81-C-5301.

[1] C. L. Chien and K. M. Unruh, Phys. Rev. B 25, 5790 (1982).

[2] N. A. Blum, K. Moorjani, T. O. Poehler and F. G. Satkiewicz, J. Appl. Phys. 52, 1808 (1981).

[3] N. A. Blum, K. Moorjani, T. O. Poehler, and F. G. Satkiewicz, J. Appl. Phys. 53, 2074 (1982).

[4] B. Window, J. Phys. E 4, 401 (1971).

[5] C. L. Chien, D. Musser, F. E. Luborsky, and J. L. Walter, J. Phys. F 10, 2407 (1978).

[6] R. L. Collins and J. C. Travis, Mössbauer Effect Methodology, Vol. 3, I. J. Gruverman, editor Plenum Press (1967), pp 123-161.

[7] J. R. Gabriel and S. L. Ruby, Nucl. Instr. Meth. 36, 23 (1965).

[8] D. J. Webb, S. M. Bhagat, K. Moorjani, T. O. Poehler, and F. G. Satkiewicz, Solid State Commun. (to be published).

[9] M. Gabay and G. Toulouse, Phys. Rev. Lett. 47, 201 (1981).